Paleoceanography and Paleoclimatology

RESEARCH ARTICLE
10.1029/2022PA004528

**Key Points:**

- PMIP4 models agree more closely with moisture-sensitive North American proxy records during the Last Interglacial than the mid-Holocene
- A subset ensemble of three models maximizes agreement and suggests sea level pressure gradient differences drove Last Interglacial precipitation patterns
- Our proxy-model comparisons offer a tool for benchmarking model skill in simulating climate states that are warmer than modern conditions

**Supporting Information:**

Supporting Information may be found in the online version of this article.

**Correspondence to:**

C. B. de Wet,
Cameron.de.wet@vanderbilt.edu

**Citation:**

de Wet, C. B., Ibarra, D. E., Belanger, B. K., & Oster, J. L. (2023). North American hydroclimate during past warms states: A proxy compilation-model comparison for the Last Interglacial and the mid-Holocene. *Paleoceanography and Paleoclimatology*, *38*, e2022PA004528. https://doi.org/10.1029/2022PA004528

Received 10 AUG 2022
Accepted 5 JUN 2023

**Author Contributions:**

**Conceptualization:** D. E. Ibarra, J. L. Oster
**Data curation:** C. B. de Wet, D. E. Ibarra, B. K. Belanger
**Formal analysis:** C. B. de Wet, J. L. Oster
**Investigation:** C. B. de Wet, D. E. Ibarra, B. K. Belanger, J. L. Oster
**Methodology:** C. B. de Wet, D. E. Ibarra, J. L. Oster
**Resources:** D. E. Ibarra, B. K. Belanger
**Software:** C. B. de Wet, D. E. Ibarra, J. L. Oster
**Supervision:** J. L. Oster
**Validation:** C. B. de Wet, D. E. Ibarra, J. L. Oster



# North American Hydroclimate During Past Warms States: A Proxy Compilation-Model Comparison for the Last Interglacial and the Mid-Holocene

**C. B. de Wet[1], D. E. Ibarra[2], B. K. Belanger[1], and J. L. Oster[1]**

[1]Department of Earth and Environmental Sciences, Vanderbilt University, Nashville, TN, USA, [2]Earth, Environmental, and Planetary Sciences, and Institute at Brown for Environment and Society, Brown University, Providence, RI, USA

**Abstract** During the mid-Holocene (MH: ~6,000 years Before Present) and Last Interglacial LIG (LIG: ~129,000–116,000 years Before Present) differences in the seasonal and latitudinal distribution of insolation drove Northern Hemisphere high-latitude warming comparable to that projected for the end of the 21st century in low emissions scenarios. Paleoclimate proxy records point to distinct but regionally variable hydroclimatic changes during these past warm intervals. However, model simulations have generally disagreed on North American regional moisture patterns during the MH and LIG. To investigate how closely the latest generation of models associated with the Paleoclimate Model Intercomparison Project (PMIP4) reproduces proxy-inferred moisture patterns during recent warm periods, we compare hydroclimate output from 17 PMIP4 models with newly updated compilations of moisture-sensitive North American proxy records during the MH and LIG. Agreement is lower for the MH, with models producing wet anomalies across the western United States (US) where most proxies indicate increased aridity relative to the preindustrial period. The models that agree most closely with the LIG proxy compilation display relative wetness in the eastern US and Alaska, and dryness in the northwest and central US. An assessment of atmospheric dynamics using an ensemble of the three LIG simulations that best agree with the proxies suggests that weaker winter North Pacific pressure gradients and steeper summer North Pacific and Atlantic gradients drive LIG precipitation patterns. Our updated compilations and proxy-model comparisons offer a tool for benchmarking climate models and their performance in simulating climate states that are warmer than present.

**Plain Language Summary** The mid-Holocene (MH) and the Last Interglacial (LIG) are the two most recent intervals that were warmer than the preindustrial and so are potentially informative analogs for future emissions scenarios. We compare the newest generation of climate models with North American precipitation patterns indicated by proxy records during the MH and LIG. We find that agreement is lower for the MH, with models producing wet anomalies across the western United States (US) where most records indicate drier conditions. Most LIG simulations show wetter conditions than the preindustrial in Alaska, northern Canada, and the southwestern US, yet the models that agree most closely with the LIG proxies also show wetness in the eastern US and aridity in the Pacific Northwest and central US. Using a subset of the three models that most closely agree with the LIG proxy records, we find that differences in LIG sea level pressure gradients in the North Pacific and North Atlantic Oceans drove shifts in the spatial and seasonal distribution of precipitation across North America. Our approach offers a strategy for assessing how well models simulate past climate during times when it was warmer than modern conditions, which may offer insight into future climate change.

## 1. Introduction

Paleoclimate proxy records aggregated for specific intervals in Earth's geologically recent past offer valuable insight into spatiotemporal patterns of hydroclimate change (PAGES Hydro2k Consortium, 2017; Tierney et al., 2020). Comparing compilations of moisture-sensitive proxies with paleoclimate model simulations can elucidate the driving mechanisms of past changes in precipitation and effective moisture (e.g., Feng et al., 2022; Harrison et al., 2003; Hermann et al., 2018; Oster et al., 2015; Otto-Bliesner et al., 2021). These comparisons are critical for assessing the ability of the current generation of models to reproduce regional hydroclimate patterns suggested by proxy records and can help inform which models may be the most useful for predictions of future moisture availability across hydrologically sensitive regions in a warmer climate state (Tierney et al., 2020).

**Writing – original draft:** C. B. de Wet, J. L. Oster
**Writing – review & editing:** C. B. de Wet, D. E. Ibarra, B. K. Belanger, J. L. Oster

Likewise, comparison of proxy records with climate models can help to refine the interpretations and clarify the biases associated with different proxy types, such as the influence of seasonality or the degree to which different timescales may be resolvable for a reconstructed climate signal (PAGES Hydro2k Consortium, 2017).

The mid-Holocene (MH) (~6,000 years Before Present (BP) and the Last Interglacial (LIG) period (~129,000–116,000 years BP) are the two most recent intervals with Northern Hemisphere temperatures comparable to those predicted by low emissions scenarios for the end of the 21st century and may offer glimpses of future hydroclimate change in regions like North America (Burke et al., 2018). Despite similar greenhouse gas concentrations as the pre-industrial (PI), the MH may have been up to 0.7°C warmer than the PI (Marcott et al., 2013). However, recent estimates using data assimilation techniques indicate that global temperatures during the MH may instead have been similar to the PI (Osman et al., 2021). Nonetheless, orbitally driven differences in the seasonal and latitudinal distribution of incoming solar radiation during the MH relative to the modern drove an enhanced seasonal temperature gradient in North America and led to strengthened Northern Hemisphere monsoons (Otto-Bliesner et al., 2017). Peak global mean LIG sea surface temperatures (127–125 ka) are estimated to have been as much as 0.9 (±0.3°C) warmer than those of the modern (Turney et al., 2020) with the greatest warming occurring in the mid- and high latitudes (Capron et al., 2017; Turney & Jones, 2010). Like the MH, the LIG had greenhouse gas concentrations roughly equivalent to the pre-industrial (Otto-Bliesner et al., 2017), but even larger seasonal differences in the distribution of insolation than the MH, which drove a warmer Arctic (Turney & Jones, 2010), smaller ice sheets, and sea level that was ~6–9 m higher than present (Dutton et al., 2015). There is evidence for considerable changes in vegetation distributions during the MH and LIG with the expansion of grassland coverage in the African Sahara (Bartlein et al., 2011; Larrasoña et al., 2013; Tierney et al., 2017), temperate forests in NH mid-latitudes (Binney et al., 2017), and boreal forests in the Arctic (LIGA Members, 1991; Muhs et al., 2001; Prentice et al., 2000).

Both the MH and LIG are included as Tier-1 experiments in the current CMIP6/PMIP4 modeling efforts, targeting the most recent interglacials to investigate the role of orbital forcing in driving climate change under conditions of comparable greenhouse gas levels to the PI (Otto-Bliesner et al., 2017). Thus, organizing updated MH and LIG proxy compilations for comparison with model output is of significant utility for the paleoclimate community, as well as for planners preparing for future warming (Tingstad et al., 2014; Woodhouse et al., 2016). Importantly, regional terrestrial precipitation and moisture balance dynamics during past warm intervals are even less well understood than temperature variations (Otto-Bliesner et al., 2021; Scussolini et al., 2019; Tierney et al., 2020), partially due to the heterogenous geographic response of the water cycle to past global climate forcing (e.g., Greve et al., 2014; Scheff, 2018), including in the western United States (Ibarra et al., 2018). Simulation of terrestrial hydroclimate can differ between Earth system models due to differences in model resolution, land-surface models of water partitioning, albedo representations and energy budget schemes, as well as complexity in cloud microphysics controlling precipitation rates, large-scale circulation patterns and orographic precipitation (e.g., Dai, 2006; Dalmonech et al., 2015; Delire et al., 2002; Trenberth, 2011). Additionally, there is insufficient data coverage for many regions for the treatment of MH and LIG vegetation distributions to be reliably constrained in PMIP4 simulations and thus the treatment of vegetation properties, changes, and feedbacks varies between models (Otto-Bliesner et al., 2021).

Here we present updated MH and LIG compilations of hydroclimate-sensitive proxy records for North America (Figure 1), where PMIP4 models produce variable regional precipitation patterns during both intervals. We statistically compare our proxy compilations with annual precipitation and precipitation minus evapotranspiration (P-ET) output from 17 individual models, as well as model ensembles, for both time slices to investigate the degree to which the latest generation of climate model simulations reproduces the moisture patterns indicated by the proxy record. We then focus on the LIG when models suggest larger hydroclimate anomalies relative to the PI and proxy-model agreement is stronger and use a subset ensemble of the three models that agree most closely with the proxies to investigate the role of atmospheric dynamics in driving precipitation patterns. Lastly, we investigate precipitation patterns predicted for the end-21st century in the models that are most successful in simulating the proxy-inferred moisture patterns for the LIG warm period and assess their similarity to LIG hydroclimate.

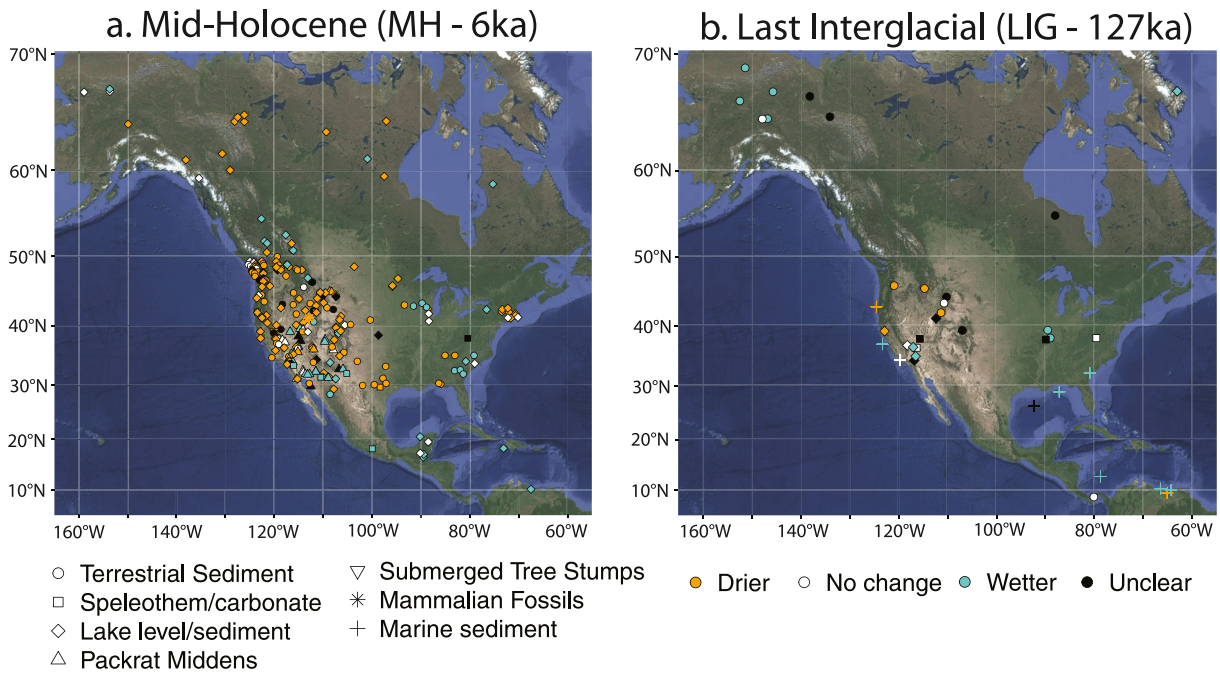


**Figure 1.** Mid-Holocene (a) and Last Interglacial (b) proxy compilations for North America designated by the type of archive (symbol) and moisture designation relative to the preindustrial for the Mid-Holocene and relative to the late Holocene/modern for the Last Interglacial (color).

## 2. Methods

### 2.1. Proxy Compilations

We compiled moisture-sensitive proxy records for the MH (Figure 1a; Table S1) and LIG (Figure 1b; Table S2) from the published literature for North and Central America (5° to 70°N, 190° to 310°W). Decades of research in the western United States (US) have resulted in dense proxy record coverage for this region during the MH, but the coverage is limited across much of Canada, the south-central US, and Central America (Bartlein et al., 1998, 2011; Hermann et al., 2018; Thompson et al., 1993). Our MH compilation includes 258 records, building on previously published regional compilations including Thompson et al. (1993) and Hermann et al. (2018) for western North America, Metcalfe et al. (2015) for the southwestern US and Mexico, Gavin and Brubaker (2015) and Steinman et al. (2016) for the Pacific Northwest, and Sundqvist et al. (2014) for Canada and Alaska. The MH compilation includes proxies from lake sediments, packrat middens, speleothems, and pollen records, as well as one record from submerged tree stumps (Lindstrom, 1990) and one of mammal fossils (Grayson, 2000).

Proxy records for the LIG are sparse and unevenly distributed in North America, with the Western US and Alaska having the best spatial coverage (Otto-Bliesner et al., 2021; Scussolini et al., 2019, 2020). This is in large part because the LIG (129,000–116,000 years BP) is beyond the limit of radiocarbon dating (~50,000 years BP), complicating the development of well-constrained chronologies for paleoclimate archives. Our LIG compilation for North America includes 39 records, expanding the work of Scussolini et al. (2019), which included 19 records from North America. Our LIG compilation consists of lake sediments, marine sediments, speleothems, landscape features, and river-cut exposures. We include two marine sediment cores from the southern Caribbean Sea as they are interpreted as representing shifts in the mean ITCZ position. For the purposes of comparison with models run for 127,000 years BP, which is likely to capture peak temperatures during the beginning of the LIG (Turney et al., 2020), we consider the part of the record that the original authors identify as the warmest part of MIS5 or MIS5e specifically to represent the LIG in our compilation.

For both time periods, we categorize proxies as recording drier (D) or wetter (W) conditions or no change (N) in annual moisture based on the original author's interpretation of the moisture signal (Tables S1 and S2). For the MH, our moisture designations are evaluated for the period 6.0 ± 1.0 ka relative to the preindustrial (PI). For the LIG, this moisture designation is made relative to the late Holocene/modern record at a given site or

within the record. For both intervals, we also include records for which no moisture signal can be interpreted due either to poorly resolved chronologies or an original interpretation of the moisture signal as representing non-local conditions, coding them as inconclusive (Figure 1). In our MH proxy compilation 55 sites are identified as wetter, 140 as drier, 38 as no change, and 25 as inconclusive. In our LIG compilation 16 proxy sites are identified as wetter, 6 as drier, and 7 as no change in moisture signal, and 10 as inconclusive. In sum, our LIG compilation contains 13 new records that were not included in the Scussolini et al. (2019) compilation and that are not designated as inconclusive, increasing the utility of the LIG proxy compilation for comparison with model output.

### 2.2. Model Output

We compare the MH and LIG proxy compilations with output of monthly climatologies from 17 PMIP4 climate models of MH (6 ka) and LIG (127 ka) simulations accessed via the World Climate Research Program (https://esgf-node.llnl.gov/search/cmip6/) between November 2020 and December 2022. Details and references for the model simulations are provided in Table S3 in Supporting Information S1. We calculate annual precipitation percent anomaly by subtracting annually averaged monthly precipitation (the CMIP6/PMIP4 variable *pr*) output for the pre-industrial (0 ka) run from either the MH (6 ka) run or the LIG (127 ka) run. We calculate annual percent P-ET anomaly by subtracting annually averaged monthly evapotranspiration output (*evspsbl*) from the annually averaged monthly *pr* output for the LIG and MH relative to the preindustrial and apply a land mask to avoid interpreting P-ET for ocean grid cells (e.g., Hermann et al., 2018; Ibarra et al., 2018; Oster et al., 2015). Since the dimensions of the resulting coastlines are dependent on the native resolution of each model and some of the MH and LIG proxy sites are near the coast or in the ocean, the number of proxy sites that are available for comparison is not consistent between models nor between precipitation and P-ET. Of the 17 models used, one (CNRM-CM6-1) provides *pr* and *evspsbl* output for the LIG but not the MH, two (MPI-ESM1-2-LR, MRI-ESM2) provide *pr* and *evspsbl* output for the MH but not the LIG, and two (NESM3, Had-GEM-GC31-LL) do not provide *evspsbl* for either timeslice. Given that *evspbl* was not available for all models and the variable sample size for the P-ET comparisons due to the required land-masking, we focus the discussion on comparison between proxy records and simulated patterns in precipitation variability, rather than changes in P-ET. To assess seasonality, we also qualitatively compare the proxy data with average precipitation percent anomalies for the MH and LIG winter half-year (NDJFMA) and summer half-year (MJJASO). We focus our quantitative comparisons on annual precipitation anomalies because a clear seasonal signal is not interpretable for the majority of proxy records. Lastly, we consider the end 21st century precipitation patterns in the models for two shared socioeconomic pathway (SSP) simulations (SSP2-4.5 and 5-8.5). We calculate end 21st precipitation anomalies for both SSP simulations by subtracting monthly averaged monthly *pr* output for the years 2071–2100 from the pre-industrial simulation in the native model resolution.

### 2.3. Agreement Coefficients

We compare hydroclimate changes observed in the proxy records (wetter, drier, no change) with the change simulated by each model at each proxy site using the Gwet's AC statistic (Equation 1) for categorical agreement between two raters (proxies and models) (Gwet, 2008, 2016). Gwet's AC accounts for agreement due to chance and is similar to Cohen's kappa ($k$), which has been used in previous studies (DiNezio and Tierney, 2013; Hermann et al., 2018). However, Cohen's kappa has been shown to underestimate true agreement when ratings are skewed toward one category (Gwet, 2016). The Gwet's AC statistic is not affected by skew across categories and has been effectively utilized in recent paleoclimate proxy-model comparison studies (Conroy et al., 2019; Feng et al., 2022). Gwet's AC is given by

$$\mathrm{AC} = \frac{P_a - P_{\mathrm{exp}}}{100\% - P_{\mathrm{exp}}} \quad (1)$$

Where $P_a$ is the percentage of agreement in sign of change between the proxies and the model output and $P_{\mathrm{exp}}$ is the expected percentage of agreement between the two due to chance alone. If models and proxy data are in complete agreement, then the AC agreement coefficient will be equal to 1. If there is no agreement between the two beyond what is expected by random chance, then the AC will be equal to 0. Opposite agreement between the models and proxy data (i.e., the model indicates wetter conditions at every site where the proxies suggest drier

and vice versa) would be represented by an AC of −1. We weight observations based on the degree of agreement between raters by multiplying a matrix of the model-proxy observations by a weight matrix in which strong agreement (e.g., both the model and proxy indicate wetter conditions at a particular site) is given a weight of 1, strong disagreement (e.g., the model indicates drier conditions, the proxy indicates wetter) is given a weight of 0, and weak disagreement (e.g., the model indicates drier, the proxy indicates no change) is given a weight of 0.5. To identify maximum possible agreement between each model and the proxy compilations we vary the threshold value for a change in *pr* and P-ET to be considered wetter or drier from 3% to 20% and 10%–50% respectively in 1% increments. For example, at a threshold of 10%, a model must simulate MH precipitation ≥110% of the PI for a site to be classified as wetter and ≤90% of the PI to be classified as drier. Based on a Student's *t*-test, most average annual precipitation and P-ET anomalies that are not significant at the 95% level ($p > 0.05$ using a Student's *t*-test) for the MH and LIG are less than 3% and 10% respectively, so we use these as the minimum precipitation and P-ET thresholds for comparison with the proxy compilations (Figure S1 in Supporting Information S1). We chose a maximum rainfall threshold of 20% because this value encompasses the range of average relative standard deviations of simulated pre-industrial annual precipitation for North American grid cells from each model.

## 3. Results

### 3.1. Mid-Holocene Proxy Compilation Observations

The moisture patterns shown by our updated MH proxy compilation ($n = 188$ records in western North America) are largely consistent with observations from Hermann et al. (2018) ($n = 170$ records) and Thompson et al. (1993) ($n = 99$) for western North America. The western US, where moisture patterns are dominated by winter westerly storm-sourced rainfall, is characterized by increased aridity during the MH relative to the PI. As in Hermann et al. (2018), central and northern California, the Pacific Northwest, and the northern Rocky Mountain regions are consistently drier than the modern, while the Great Basin and southern Rockies exhibit a mixture of sites indicated wet, dry, and unchanged conditions (Figure 1a). Areas in the southwestern US and northern Mexico where the North American Monsoon contributes significantly to annual rainfall also show a mixed response. Most sites along the US-Mexico border indicate increased MH wetness, whereas sites from northern New Mexico and northern Arizona suggest enhanced aridity.

Modern precipitation patterns become less highly seasonal to the east of the Rocky Mountains and western Great Plains, with a roughly equal distribution of summer and winter moisture (Lora & Ibarra, 2019; PRISM Climate Group, 2020). MH proxy records from the Plains region in Texas and the Florida Panhandle demonstrate aridity ($n = 8$), as do several records from southern New England ($n = 10$). Meanwhile, records from the Carolinas and coastal Georgia indicate greater wetness during the MH ($n = 6$). A collection of sites in the upper Midwest shows a mixed response ($n = 9$). All the sites that we include from the Yucatan Peninsula, Central America, and the Caribbean region indicate wetter conditions or no change ($n = 10$). In Canada, southern British Columbia was drier along the border with the US ($n = 5$), with wetter conditions further north ($n = 5$). Drier conditions are observed in the Yukon and the Northwest Territories, and southern Nunavut ($n = 12$), aside from one wetter site in central Canada. Records from Alaska display a mixed response with two showing no change, one wetter, and one drier ($n = 4$).

### 3.2. Mid-Holocene Proxy—Model Comparisons

Overall, agreement between the MH proxy compilation and model simulations is low for both annual precipitation (Figure 2b, Figure S2 in Supporting Information S1) and P-ET (Figure S3 in Supporting Information S1). The full PMIP4 MH ensemble produces a maximum AC value of 0.23 for precipitation at thresholds of 11%–20% (Figure 2a). Fourteen of the 16 models that provide MH output produce AC values between 0.19 and 0.24, with optimized rainfall thresholds that range from 7% to our maximum value of 20%, and nine of the 16 models are optimized at a threshold of 16% or higher (Figure 2b). These simulations show wetter MH conditions relative to the PI along the western US-Mexico border, where proxies also indicate enhanced wetness. However, most models also show some pattern of enhanced wetness over all or part of California, the Great Basin, the Pacific Northwest, and the Colorado Plateau, where a high concentration of proxies indicate enhanced MH aridity. Since the wet anomaly in the simulations tends to be relatively modest (generally less than 20% wetter than the PI) our algorithm maximizes agreement by increasing the rainfall threshold such that most western US dry sites are

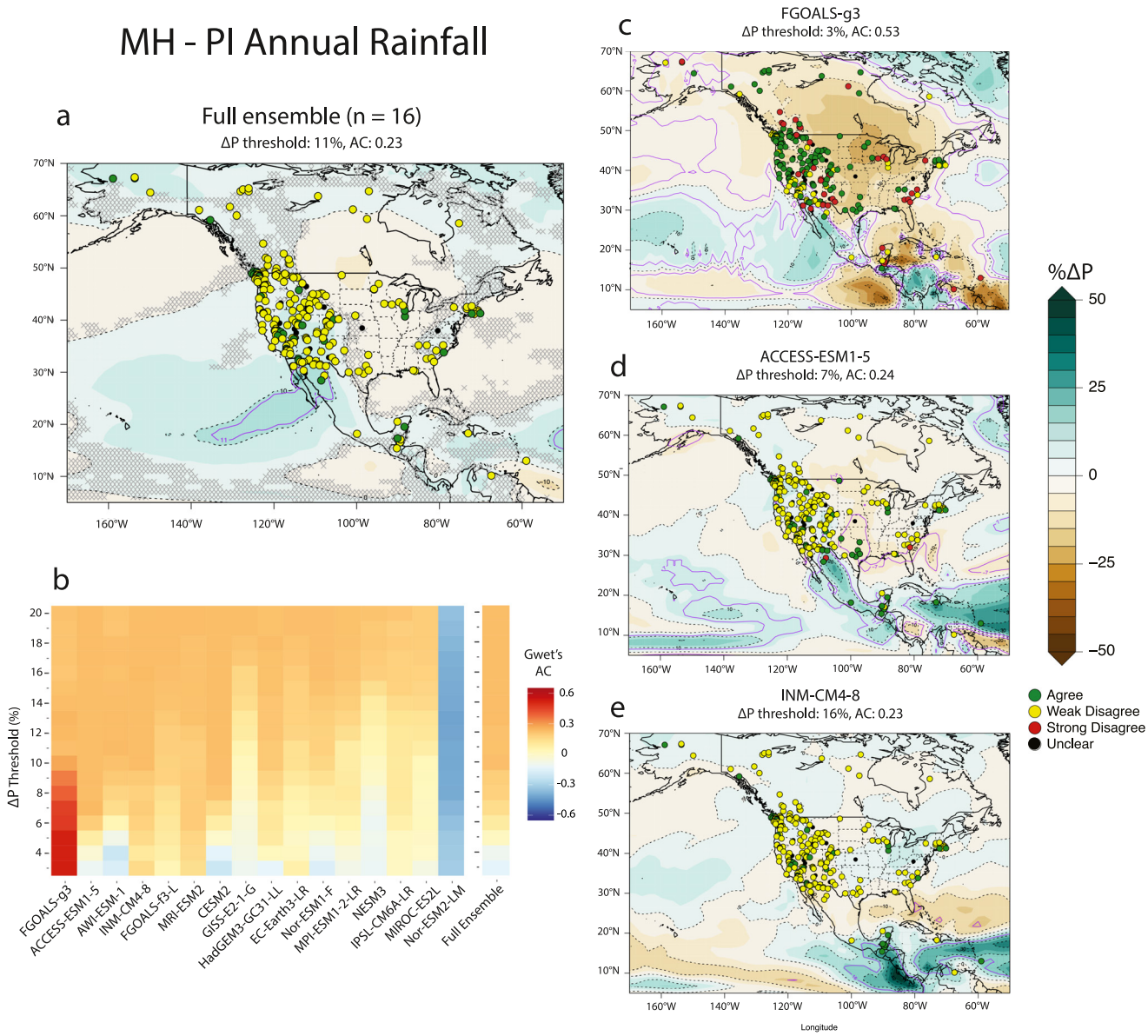


**Figure 2.** (a) Annual MH-PI precipitation anomaly (%ΔP) for the full PMIP4 ensemble ($n = 16$) with MH proxy compilation plotted based on agreement with the ensemble climatology. (b) Heat map showing AC values at each threshold (3%–20%) for the MH-PI annual precipitation anomaly to be considered wetter, drier, or unchanged. Higher AC values indicate better model-proxy agreement. (c, d) Annual MH-PI precipitation anomaly (%ΔP) with MH proxy compilation plotted based on agreement with the underlying model climatology for the three models with the highest maximum AC values (c: FGOALS-g3, d: ACCESS-ESM1-5, e: AWI-ESM-1). Solid purple lines denote the threshold for the change in precipitation to be considered wetter, drier, or unchanged based on optimized agreement with the proxy compilation. Dashed lines denote contour intervals of ±0%, 10%, 20%, 30%, and 40%. Hatching in (a) indicates regions where more than one third of models disagree in the sign of precipitation change.

categorized as weakly disagreeing with the lack of significant hydroclimate change in most of the simulations. Thus, the MH simulations for which agreement in the western US is optimized by increasing the precipitation threshold also tend to produce weak disagreement with wetter or drier archives across other regions in North America where modeled changes are small, such as the eastern US and Great Plains. One model, Nor-ESM2-LM, produces a large wet anomaly along the western coast of Canada that extends down into the western US, driving widespread disagreement with the proxy compilation and negative AC value (Figure S2 in Supporting Information S1).

FGOALS-g3 stands out in our MH precipitation comparisons with an AC value of 0.53 at a threshold of 3% and 0.52 or higher at a threshold of 5% or less (Figure 2c). This is driven by widespread aridity in the model

across most of the US and Canada and thus good agreement with the large concentration of "drier" proxy sites in the western US. Additionally, FGOALS-g3 produces wet anomalies in southern California and southwestern Arizona, driving good agreement with the wetter archives along the western portion of the US—Mexico border. However, this wet anomaly in the simulation does not extend east to the numerous wet sites in southeastern Arizona, northern Mexico, and southern New Mexico. Indeed, the rest of the US and most of Canada are characterized by aridity, driving agreement with concentrations of drier proxy sites in Texas, the northeast, and parts of the Midwest, as well as northwest Canada, but disagreement with the enhanced wetness of the Yucatán Peninsula, southeast US, and southern Wisconsin.

The range of agreement between the MH proxy records and simulated annual average P-ET is comparable to precipitation (Table S4 and Figure S3 in Supporting Information S1). Like precipitation, most MH simulations show wet anomalies in P-ET across the western North America and patterns of aridity in some or most of Canada and the central US. Nine of the 14 models that provide *evspsbl* output produce maximum AC values between 0.11 and 0.24. The other 5 are below 0.1. In contrast to the AC results for precipitation, FGOALS-g3 does not display better agreement than other simulations for P-ET, with an AC value 0.16 at a high threshold of 42%.

### 3.3. Mid-Holocene Seasonal Patterns

At least two thirds of the models in the MH ensemble display wet precipitation anomalies across the western US in the winter and in the southwest US during the summer half-year (Figure S6 in Supporting Information S1). The MH ensemble shows dry anomalies in the Pacific Northwest during the summer, which may align with the high concentration of dry proxies in the region, but the magnitude is small (<10%) and more than one third of models disagree on the sign of this change. FGOALS-g3 is characterized by strong summer aridity and weak winter aridity across most of North America with winter wet anomalies in Mexico and the southwest. Qualitatively, these patterns align well with the aridity in most MH proxy records, and the winter wetness in the southwest may help explain the wet proxy signal along the US-Mexico border. However, without a reliable understanding of seasonal signals in the proxy records, which is not adequately available in the literature, we are unable to carry out quantitative comparisons on a seasonal basis.

### 3.4. Last Interglacial Proxy Compilation Observations

There are fewer records in the compilation for the LIG than for the MH. LIG proxy records from the western US document drier conditions across the Pacific Northwest and northern Rockies and increased wetness in the southwest (Figure 1b; Table S2 and references therein). Terrestrial pollen from marine sediment cores indicates drier conditions along the Oregon coast and wetter conditions or conditions similar to today along the California coast (Heusser, 2000; Lyle et al., 2010; Pisias et al., 2001). Lake records from the western US track vegetation changes and shifts in water levels, with lakes from the northern US Rocky Mountains (Jiménez-Moreno et al., 2007), the Pacific Northwest (Whitlock & Bartlein, 1997), and northern California (Adam & West, 1983) indicating relative aridity during the LIG, while Great Basin lakes document wetter conditions or conditions similar to the present (Forester et al., 2005; Reheis et al., 2012; Woolfendon, 2003). Other lake records from the Rocky Mountains (Anderson et al., 2014; Baker, 1986; Balch et al., 2005; Miller et al., 2014; Sharpe & Bright, 2014) and southern California (Glover et al., 2017) do not display clear signals of LIG hydroclimate.

We identify four Alaskan proxy sites across the central and northern portions of the state that indicate wetter LIG conditions (Bigelow et al., 2014; Bigelow et al., 2014; CAPE Last Interglacial Project Members, 2006; Muhs et al., 2001), as well as one that indicates no change in moisture (Pewe et al., 1997). We also identify two sites that suggest warmer, but not necessarily wetter conditions in the Yukon region of western Canada (Schweger & Matthews, 1991; Tarnocai, 1990). There are relatively few LIG records available for the rest of mainland Canada, likely due to the erosive nature of the Laurentide ice sheet during the last glaciation (LIGA Members, 1991). We identify one record from the Hudson Bay lowlands that is suitable for inclusion in our compilation based on the continuous chronology, but which displays an uncertain climate signal at the LIG (LIGA Members, 1991; Wyatt, 1990).

Of the few LIG proxy records that exist from the eastern US, the majority indicate increased moisture. However, the poor proxy record coverage limits our ability to make broad-scale interpretations of hydroclimate changes for this region. Pollen records from two southern Illinoisan lakes have been interpreted as indicative of wetter

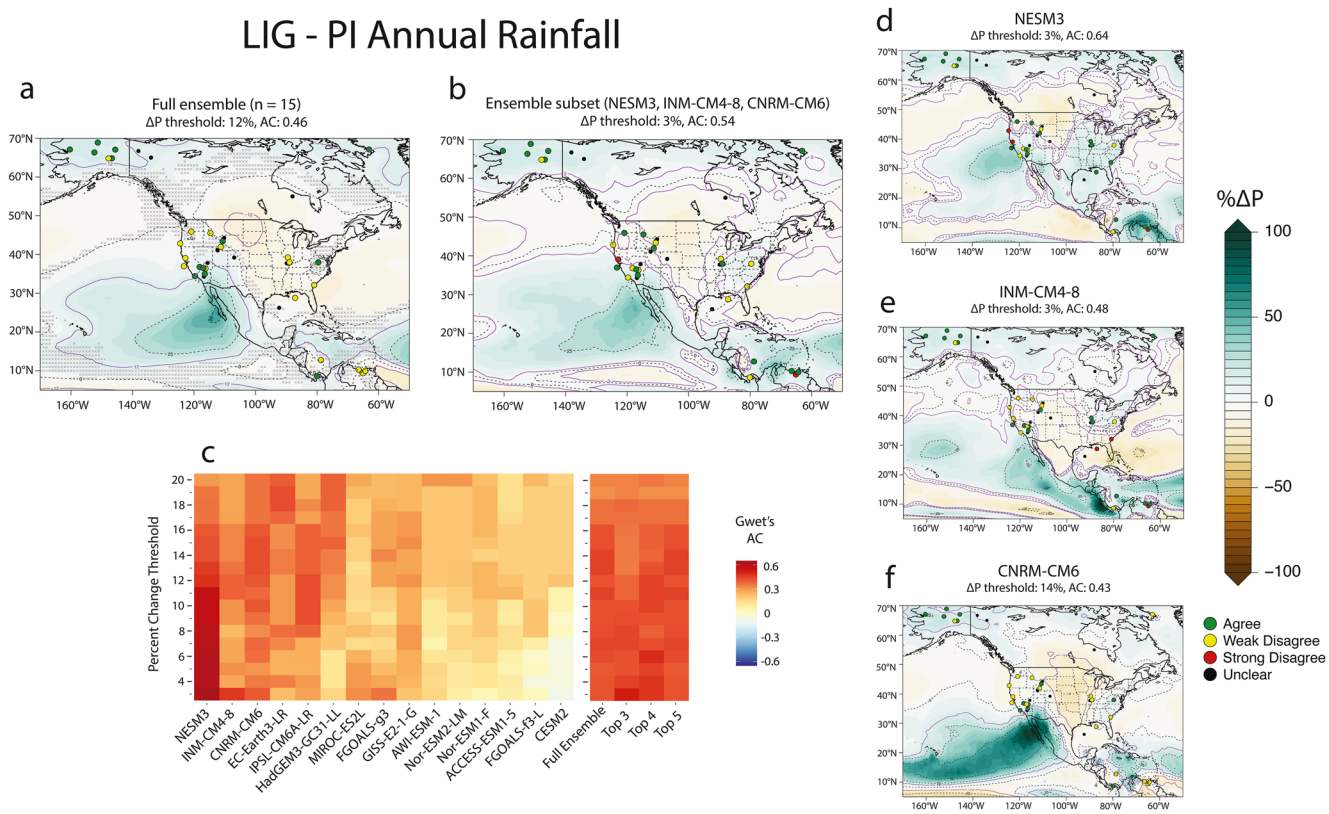


**Figure 3.** (a) Annual LIG-PI precipitation anomaly (%ΔP) for the full PMIP4 ensemble ($n = 15$) with LIG proxy network plotted based on agreement with the ensemble climatology. (b) Annual LIG-PI precipitation anomaly (%ΔP) for the full ensemble subset of the three models that agree most closely with the LIG proxy network. (c) Heat map same as in Figure 2 for LIG-PI, including AC values for the full PMIP4 ensemble and ensembles of the top three, four, and five models in terms of agreement with the LIG proxy network. (d–f) Same as Figure 2 for three models in the ensemble in b. (d: NESM3, e: INM-CM4-8, f: CNRM-CM6). Purple solid lines and hatching same as in Figure 2. Dashed lines denote contour intervals of ±0%, 25%, 50%, and 75%.

conditions relative to the present (Curry & Baker, 2000; Teed, 2000), as have terrestrial inputs in marine sediment cores from northern Gulf of Mexico and the coast of South Carolina and Georgia (Limoges et al., 2014; Suh et al., 2020).

Changes in geochemistry and mineralogy in marine sediment core MD02-2549 from the north central Gulf of Mexico indicates a northeast migration of the main rainfall belt over the Mississippi River basin in response to greater boreal summer insolation of the LIG (Montero-Serrano et al., 2011). While this hypothesis is consistent with the increased wetness observable in Illinoisan lakes (Curry & Baker, 2000; Teed, 2000), we opt to code this core site as unclear in our proxy compilation because the signal interpreted by Montero-Serrano et al. (2011) is highly non-local. Additionally, two LIG speleothem records show no change in moisture conditions in western Virginia (Springer et al., 2014) and an inconclusive moisture signal in southeastern Missouri (Knight et al., 2006).

We identify one Central American soil record and two Caribbean Sea marine sediment cores that meet our criteria for inclusion in the LIG compilation. Pollen data from the soil record of El Valle, Panama is indicative of hydroclimate conditions similar to that of today (Cárdenes-Sandí et al., 2019), while the proximal ODP Core 999A has been interpreted as indicating wetter conditions at the LIG (Schmidt & Spero, 2011), though Scussolini et al. (2019) note that the signal is weak, and uncertainty is large in the record. Riboulleau et al. (2014) interpret sedimentological variations in a Cariaco Basin core to indicate more or less rainfall over different river basins in Venezuela during the LIG. Here we adopt the approximate locations of the river basins from Scussolini et al. (2019) for the purpose of plotting the sign of change at the sites.

### 3.5. Last Interglacial Proxy—Model Comparisons

Agreement between the proxy compilation and model simulations is greater for the LIG than for the MH for both precipitation (Figure 3c, Figure S4 in Supporting Information S1) and P-ET (Figure S5 in Supporting Information S1). The LIG ensemble ($n = 15$) produces an AC value of 0.46 at an intermediate rainfall threshold of 12% (Figure 3a), which is a higher degree of agreement than 13 of the 15 individual models (Figure 3c). The model NESM3 produces the highest degree of agreement with the proxy compilation, with an AC value of 0.64 at a rainfall threshold of 3% (Figure 3d). The model INM-CM4-8 (Figure 3e) displays the second highest value of 0.48 at rainfall thresholds of 3%. The models CNRM-CM6 (Figure 3f), EC-Earth3-LR, and IPSL-CM6A-LR display AC values of 0.43 at thresholds of 13%–15%, 18 or 19%, and 9%–12% respectively. Most other models are optimized at rainfall thresholds between 12% and 20% and display AC values that range from 0.21 to 0.39 (Figure 3c).

Our LIG comparisons expand upon previous work by Scussolini et al. (2019), who show agreement between their proxy compilation and model ensemble ($n = 7$) on increased LIG rainfall in Alaska and northern South America, but an ambiguous relationship across the contiguous US. Similarly, we observe weak disagreement between our LIG ensemble ($n = 15$) and expanded LIG proxy compilation in much of the US (Figure 3a). Increased precipitation in Alaska and the southwest US, where LIG proxies indicate wetter conditions, is relatively consistent across all models and in the ensemble (Figure 3). Most models and the ensemble also show a domain of enhanced LIG aridity in the Great Plains, though there are no LIG proxy sites in this region for comparison. There is disagreement among models in the sign of rainfall change across much of the rest of North America, though the magnitude of anomaly tends to be smaller than in the southwest US or northern Great Plains (Figure S4 in Supporting Information S1). The LIG ensemble is characterized by a transition between wetness in the west and aridity in the Midwest and east that runs from southeastern New Mexico through Idaho, though the magnitude of anomaly across these regions is below the optimized rainfall threshold of 12%. This pattern drives weak disagreement with the drier proxy records distributed across the Pacific Northwest and Rocky Mountain region and with the wetter records of southern Illinois, the Gulf of Mexico, and the coastal southeast US.

We find that an ensemble of three of the models that most closely agree with the LIG proxy compilation—NESM3, INM-CM4-8, and CNRM-CM6—maximizes agreement with the LIG proxy compilation relative to any other individual model aside from NESM3 or combination of models, including those with EC-Earth3-LR and IPSL-CM6A-LR (Figure 3b). This subset ensemble displays an AC value of 0.54 at an optimized rainfall threshold of 3%. Agreement with the wetter proxy sites in Alaska and southern California is consistent between the subset ensemble ($n = 3$) and full ensemble ($n = 15$). However, the subset ensemble shows better agreement with drier proxy sites in the Pacific Northwest and in the Rocky Mountains, where it displays low magnitude, but robust dry anomalies. The low magnitude wet anomalies in the full ensemble are below the optimized rainfall threshold, driving weak disagreement with all but the Porcupine Creek record of western Wyoming which has been interpreted as representing moisture conditions similar to the present day (Pierce et al., 2011). The subset ensemble also aligns more closely with the wetter proxy sites of southern Illinois in the Midwest US and of the Gulf of Mexico and the coastal southeast US, all of which are situated close to the wet-dry anomaly transition, likely contributing to the low optimized rainfall threshold of the subset ensemble. Thus, our subset ensemble may help reconcile disagreement between the aridity in the Mississippi River Basin of the full LIG ensemble and LIG proxies in southern Illinois, which indicate enhanced LIG rainfall. Finally, the subset shows a wetter southern Caribbean, where three of the five records in our compilation are wetter, compared to the ambiguous climatology of the full ensemble.

AC values calculated for comparisons between the LIG proxy records and simulated annual average P-ET are slightly higher than those for simulated precipitation (Table S5 and Figure S5 in Supporting Information S1). Similar to precipitation, the models show wetter LIG P-ET conditions in Alaska, Mexico, and the southwest US with some pattern of drier P-ET conditions in eastern Canada and the central US. Some models show this aridity extending to the eastern US while others produce spatially variable patterns of wetter P-ET conditions along the east coast of the US. CNRM-CM6 produces the highest AC value for LIG P-ET with 0.55 at a threshold of 16%. Ten of the 12 models that provide *evspsbl* output for the LIG produce maximum AC values between 0.46 and 0.32 across a wide range of thresholds. *Evspsbl* output was not available for NESM3, the model with the highest agreement for LIG precipitation, at the time of publication.

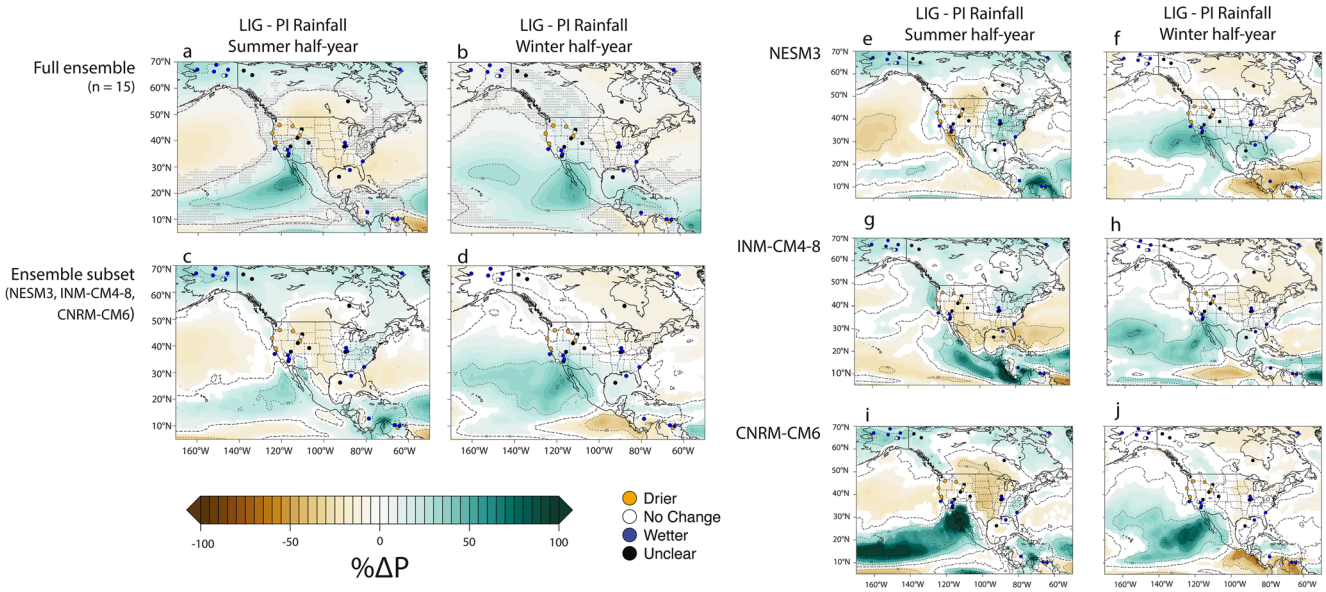


**Figure 4.** Summer (MJJASO) and winter (NDJFMA) half-year LIG—PI rainfall anomalies for the full PMIP4 ensemble (a and b), the ensemble subset (c and d), and the three models that make up the ensemble subset (NESM3: e and f; INM-CM4-8: g and h; CNRM-CM6: i and j). Proxy sites are plotted based on rainfall designation at the LIG relative to the PI. Anomalies that are not significant at the 95% level ($p > 0.05$ using Student's *t*-test) are omitted from the plots in c–j. Dashed lines and hatching same as in Figure 3.

### 3.6. Last Interglacial Seasonal Patterns

Individual PMIP4 simulations display variable responses to the enhanced seasonality that was driven by the orbital forcing of the LIG. We avoid quantitative comparisons between models and proxies on a seasonal basis because seasonal biases in LIG proxy records are often unclear, speculative, or in development in the paleoclimate proxy literature (Kwiecien et al., 2022 and references therein). Rather, we compare the subset of models that maximize annual agreement with the LIG proxy compilation (Figures 4c and 4d) with the full PMIP4 ensemble (Figures 4a and 4b) to help elucidate some of the seasonal patterns in North American LIG rainfall.

The ensemble subset and full ensemble display some similarities in the seasonality of precipitation anomalies. During the LIG summer half-year both the full ensemble and the ensemble subset are characterized by wetter conditions across Alaska, northern Canada, and Mexico and drier conditions in southern Canada, the central US, and the Pacific Northwest (Figures 4a and 4c). Both show enhanced aridity in eastern Canada, the northern Great Plains, and northeast US and wetter conditions in the southwestern US and Mexico during the winter half-year (Figures 4b and 4d). However, key differences exist between precipitation seasonality in the full and subset ensembles, which may help explain the precipitation patterns suggested by the proxy records. During the winter half-year, the subset ensemble shows increased rainfall in the southeastern US and a mix of wet and dry conditions along the northwest coast of the US and Canada, whereas the full ensemble indicates aridity in the southeastern US and wetness along the northwest coast of US and Canada (Figures 4b and 4d). The subset ensemble also displays more widespread wet conditions in the eastern US and in northern South America during the summer half-year relative to the full ensemble (Figures 4a and 4c).

Additionally, the subset ensemble differs from the full ensemble in terms of the seasonal pattern of wet anomalies in the North American Monsoon (NAM) region. While many models show a positive annual rainfall anomaly in the southwestern US, a closer look at the spatial distribution and seasonal balance of rainfall between models indicates that different mechanisms drive this annual anomaly in each model (Figure 4). The annual increase in rainfall in the southern US may result from an expanded and strengthened NAM, a strengthened, but not significantly expanded monsoon, or an increase in southwesterly winter rainfall. Scussolini et al. (2019) observe a wetter and moderately expanded NAM in their LIG ensemble climatology, though there is considerable inter-model spread that hinders a more conclusive understanding of how far into California and/or the Great Basin this anomaly extends. Similarly, our full ensemble shows enhanced summer half-year rainfall occurring from southern California into the southern Great Basin and as far east as central New Mexico (Figure 4a). The subset

ensemble differs from the full ensemble in that it is characterized by a summer half-year rainfall anomaly that extends northward from Mexico but is localized to Arizona within the US and does not extend west to the wetter LIG proxy sites of southern California (Figure 4c). Taken individually, there is disagreement among the top three models in the spatial distribution of summer moisture in the southwestern United States. NESM3 shows enhanced rainfall across Mexico and into Arizona and New Mexico (Figure 4e). INM-CM4-8 displays an opposite response, showing enhanced summer aridity across the NAM domain, including northern and central Mexico (Figure 4g). CNRM-CM6 shows greatly enhanced rainfall in southern California and Arizona that extends northward into southern Nevada (Figure 4i). A lack of resolvable proxies in northern Mexico, Arizona, and New Mexico, as well as the southern Rockies, makes specific interpretations about the geometry of the NAM domain during the LIG challenging. The development of new proxy records from these climatologically important but currently unrepresented locations will be key for generating a better understanding of the characteristics of regional precipitation patterns during the LIG, like the NAM. The three models included in the ensemble subset are in much closer agreement with regard to cool season rainfall, with all three showing enhanced wetness across the southwest US during the winter half-year (Figures 4f, 4h and 4j).

### 3.7. Atmospheric Dynamics During the Last Interglacial

To assess the atmospheric drivers of LIG moisture patterns, we present sea level pressure (SLP) and 850 hPa wind vector output for the ensemble of the three models that agree most closely with the LIG proxy record (Figure 5).

During the winter half-year, the ensemble subset LIG NPH is weaker and less longitudinally expansive, and the AL is less deep in the Gulf of Alaska but extends further west along the Aleutian Island chain relative to the PI (Figures 5b, 5d and 5f). Correspondingly, the gradient between the AL and NPH is weaker during the LIG winter (Figure 5g), as illustrated by the large negative winter SLP pressure anomaly in the central Pacific between 20 and 50°N and the associated strong cyclonic surface wind vector anomalies (Figure 5f). The LIG SLP anomalies in the Gulf of Mexico and Atlantic Ocean during the winter half-year are lower magnitude than those of the Pacific Ocean. We observe slightly higher LIG subtropical Atlantic SLPs and lower SLPs in the northern Atlantic (Figure 5f) driving a moderate strengthening of the LIG latitudinal SLP gradient (Figure 5h).

During the LIG summer half-year the ensemble subset produces a stronger and more expansive NPH and lower SLPs across Alaska, Canada, and most of the contiguous US relative to the PI (Figures 5a, 5c and 5d). This results in a steeper LIG latitudinal pressure gradient (Figure 5g) and strong anticyclonic surface wind vector anomalies in the north Pacific relative to the PI (Figure 5e). The Atlantic Ocean is characterized by negative pressure anomalies in the subtropics and high latitudes (>50°N) during the LIG summer half-year relative to the PI (Figure 5e) and a LIG SLP gradient that is shifted northward and lower in magnitude than that of the PI (Figure 5g).

### 3.8. Projected North American Hydroclimate in Shared Socioeconomic Pathway Simulations

End 21st century precipitation anomalies from two SSP scenarios—SSP2-4.5 (+4.5 W $m^{-2}$; medium forcing pathway) and SSP5-8.5 (+8.5 W $m^{-2}$; high-end forcing pathway)—calculated relative to the PI using the models in our ensemble subset that agrees most closely with LIG proxy records are shown in Figure 6 and compared with LIG hydroclimate patterns in Section 4.3. On an annual basis the ensemble subset predicts increased precipitation at the end of the 21st century relative to the PI across Alaska, Canada, the Pacific Northwest, the Great Lakes region, and the eastern US and decreased precipitation in Mexico, Texas, and the southwestern US for the SSP2-4.5 scenario (Figures 6a–6c). Precipitation anomalies of greater magnitude but the same spatial pattern are projected for the SSP5-8.5 scenario in the subset ensemble (Figures 6d–6f). These findings are largely consistent with those from the model ensemble ($n$ = 13) produced by Cook et al. (2020) who observe robust wetting in Alaska, Canada, and the eastern US and drying in western and southern Mexico and Central America, but non-robust changes in the central and western US.

During the summer half-year, the ensemble subset predicts relatively more arid conditions across the already water-sensitive western US in the SSP2-4.5 simulations (Figure 6b). During the winter half-year arid conditions in the ensemble subset are projected in Mexico and extending northward into Texas, Arizona, New Mexico, and southern California (Figure 6c). The magnitude of these patterns is even greater for the SSP5-8.5 simulation (Figures 6e and 6f). Outside of these regions the ensemble subset shows mostly positive North American rainfall anomalies at the end of the 21st century, especially in the higher latitudes (Figures 6b, 6c, 6e, and 6f).

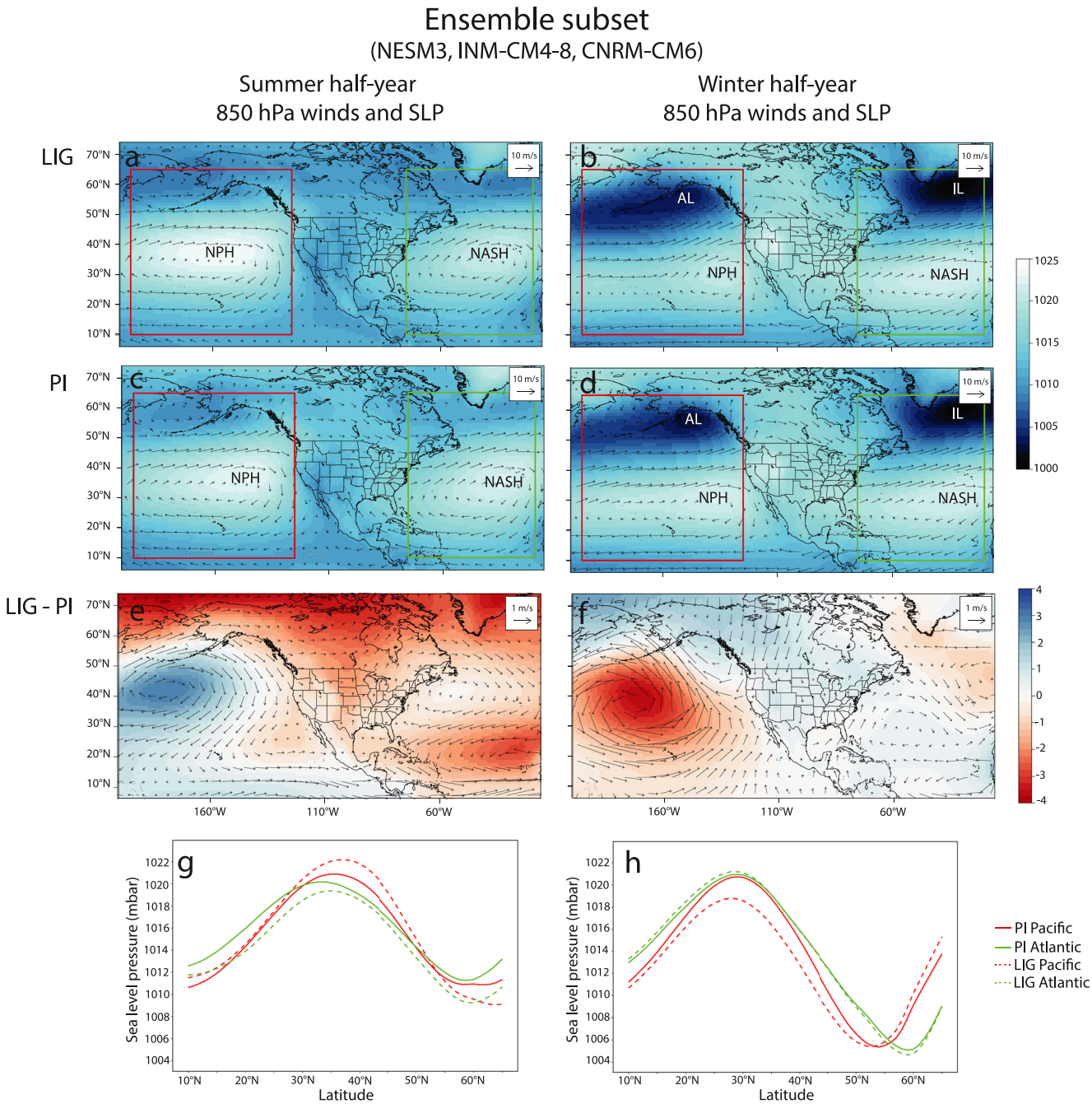


**Figure 5.** Ensemble subset summer half-year and winter half-year 850 hPa wind vectors and sea level pressure for the LIG (a, b), PI (c, d), and LIG-PI anomaly (e, f). Latitudinal pressure gradient for 10° to 65°N zonally averaged from 165° to 235°W in the Pacific Ocean (red box in a–d) and from 75° to 20°W in the Atlantic Ocean (green box in a–d) for the LIG and PI. AL: Aleutian Low. NPH: North Pacific High. IL: Icelandic Low. NASH: North Atlantic Subtropical High.

## 4. Discussion

### 4.1. Progress and Considerations for Mid-Holocene Proxy-Model Comparisons

Our finding of low overall agreement between the expanded North American proxy compilation and MH simulations is consistent with previous analyses of earlier PMIP simulations which found that models produce opposite sign and/or smaller magnitude MH precipitation anomalies in North America than are suggested by paleoclimate proxy reconstructions (Braconnot et al., 2012; Harrison et al., 2015, 2016; Hermann et al., 2018). FGOALS-g3 displays the highest degree of agreement, largely driven by widespread MH dry annual anomalies in western

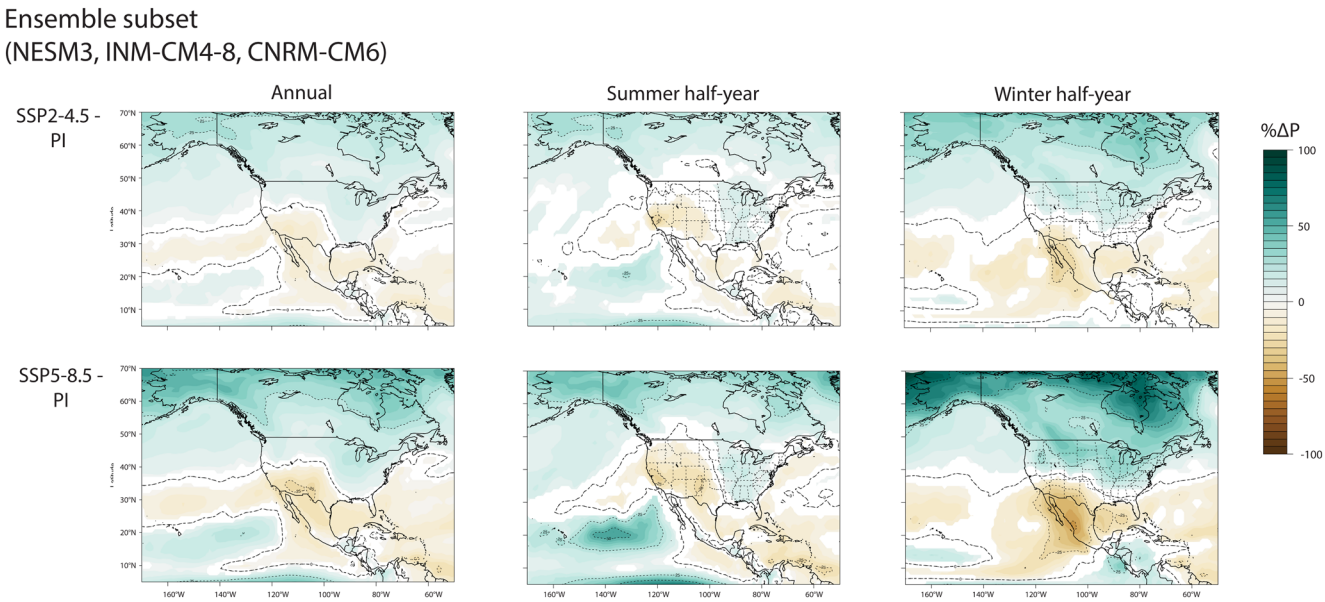


**Figure 6.** Annual, summer (MJJASO) and winter half-year (NDJFMA) precipitation anomalies (% change, 2071–2100 vs. the pre-industrial) for the SSP2-4.5 (a–c) and SSP5-8.5 (d–f) simulations in the ensemble subset. Anomalies that are not significant at the 95% level ($p > 0.05$ using Student's $t$-test) are omitted from the plots. Dashed lines same as in Figure 3.

North America where there is a high concentration of proxies that indicate aridity. These dry anomalies were also present in the earlier FGOALS-g2 simulation, leading to higher proxy-model agreement than other PMIP3 models (Hermann et al., 2018).

In most cases, our algorithm for choosing a MH precipitation threshold to optimize AC results in large thresholds, widespread weak disagreement with any proxy site that is coded as wetter or drier, and a clustering of AC values between 0.19 and 0.23. This makes it difficult to differentiate between models in terms of agreement with our expanded proxy compilation, despite considerable variability in the pattern of precipitation anomalies across North America between model simulations. It is possible that MH proxies are responding in a non-linear way, recording signals of increased aridity in response to small changes in actual rainfall, or are being interpreted here and in past literature as annual signals when they are in fact biased toward anomalies present only in particular seasons. Further investigations into proxy seasonality and the thresholds of proxy response to environmental changes may assist in accounting for proxy bias in these comparisons.

Alternatively, the MH hydroclimate patterns suggested by the proxy compilation may reflect processes such as climate-vegetation feedbacks that are not fully represented in the model simulations. Changes in vegetation can influence climate via changes to water cycling, surface albedo, and dust mobilization and can drive different dynamical circulation patterns than those expected from orbital, greenhouse gas, and ice sheet forcings alone (e.g., Thompson et al., 2022). Since the differences in orbital forcing and other CMIP6/PMIP4 boundary conditions between the MH and PI are relatively small, especially compared to those of the LIG, these finer-scale emergent climate feedbacks, such as vegetation response to seasonally biased MH warming, may be especially important for the precipitation dynamics of the MH. For example, vegetation feedbacks for a "Green Sahara" during the MH have been shown to enhance tropical cyclone activity (Pausata, Emanuel, et al., 2017), suppress El-Niño Southern Oscillation (ENSO) activity (Pausata, Zhang, et al., 2017), and intensify the Northern Hemisphere monsoon precipitation (Sun et al., 2019). These and other investigations, such as including expanded Eurasian forest cover in MH models (Swann et al., 2014), have helped resolve mismatches between simulated and observed precipitation response on a global scale (Pausata, Emanuel, et al., 2017; Pausata, Zhang, et al., 2017; Piao et al., 2020; Sun et al., 2019; Tabor et al., 2020).

While dynamical treatment of vegetation remains a challenge for Earth system models of past and present climates, it may contribute to the mismatch between our North American proxy compilation and the CMIP6/PMIP4 simulations. None of the MH simulations include fully dynamic vegetation and the few that include

interactive vegetation do not stand out in the quality of comparison with the MH proxy compilation (Table S3 in Supporting Information S1). Additionally, the CMIP6/PMIP4 simulations do not appear to have improved in the simulation of extratropical circulation relative to CMIP5/PMIP3 (Brierley et al., 2020), an issue that has been pinpointed as a likely cause of mismatches between simulated and observed moisture patterns in Eurasia (Bartlein et al., 2017) and Europe (Mauri et al., 2014) and one that may play an important role for North America as well. The persistent mismatch between the modest MH rainfall anomalies of PMIP simulations and the patterns evident in MH proxy networks deserves further consideration.

### 4.2. Drivers of North American Hydroclimate During the Last Interglacial

The radiative forcing during the LIG was similar to that of the MH, but stronger (Otto-Bliesner et al., 2017), and the pattern of hydroclimate response is similar between the two PMIP4 ensembles. Of the few proxy records that meet the criteria to be considered in both the MH and LIG compilation, the majority display the same sign of precipitation change during both intervals relative to the PI. So, the dynamical drivers that we investigate for LIG hydroclimate may also be relevant for the MH. However, it may be the case that agreement is higher for the LIG simulations because the orbitally driven insolation forcing is larger than during the MH and thus other climate feedbacks like vegetation responses, which are not fully included in the models, may be relatively less influential on LIG hydroclimate patterns overall. We focus our discussion of the drivers of hydroclimate change on the LIG because of the larger simulated hydroclimate response during this interval relative to the MH and because the agreement between the models and the proxy records is higher overall, and especially so for the models that we include in the ensemble subset.

Interactions between the semi-permanent pressure systems over the Pacific and Atlantic play a large role in the amount and seasonal distribution of precipitation across much of North America (e.g., Wise, 2016). Specifically, the location and relative strength of the North Pacific High (NPH) and Aleutian Low (AL) are relevant for the geometry of winter storm tracks that deliver moisture to Alaska and the western US, where there is a large concentration of LIG proxy sites (e.g., Oster et al., 2015; Swain et al., 2014; Wong et al., 2016). In the eastern US, the gradient between low SLP in the subtropical Atlantic Ocean and high SLP in the north Atlantic and the position of the North Atlantic Subtropical High (NASH) and has been shown to play a large role in the amount and source of rainfall during both the modern (Diem, 2013; Labosier & Quiring, 2013; Li et al., 2011) and the Holocene (Hardt et al., 2010), including via the incidence of summer tropical cyclones along the Gulf Coast and east coast of North America (e.g., Baldini et al., 2016). An assessment of how these pressure systems differed under the enhanced seasonality of the LIG relative to the PI may thus provide insights into the mechanisms driving the spatial patterns and seasonal distribution of LIG rainfall.

In the southwestern US, where enhanced rainfall is shown in the ensemble subset and by the proxy records, the slackened SLP gradient in the Pacific may have allowed for more westerly storms to penetrate the continent during the LIG, driving fewer large-scale droughts and the overall wetter winter half-year conditions relative to the PI. This pressure configuration is largely inverse to that which characterized western US-wide droughts over the last 500 years (Wise, 2016). These dry intervals are characterized by a strong AL, anomalously low pressure over eastern North America, and an intense high-pressure ridge centered over the Pacific Northwest, which would block storms from penetrating into the Western US and enable prolonged dry conditions. The model simulations indicate that these pressure conditions may have been less pervasive on average during the LIG winters, which could explain the enhanced southwestern US wetness simulated by the models and shown by proxy records.

The steeper LIG latitudinal pressure gradient (Figure 5g) and strong anticyclonic surface wind vector anomalies in the north Pacific relative to the PI during the LIG summer half-year (Figure 5e), along with a strengthening of the jet stream (Figure S8 in Supporting Information S1), may have facilitated greater moisture delivery to the Alaska interior and western Canada, where the ensemble subset indicates enhanced wetness (Figure 4c). To the south, where the jet stream is relatively weaker during the LIG, the wet LIG anomalies do not extend past the west coast of the US, which may be related to the westward expansion of the NPH and the corresponding enhancement of southward meridional wind vector anomalies in the east Pacific that do not penetrate the continental interior. Thus, a key finding of this work is that while the NAM may have been strengthened it was perhaps not significantly expanded during the LIG and that the enhanced annual wetness of the southwestern US was instead driven primarily by increased southwesterly wintertime rainfall as opposed to summertime monsoonal rainfall.

The ensemble subset winter half-year moisture signal is less clear in northwestern NA, with low magnitude wet anomalies in eastern Alaska and low magnitude dry anomalies in British Columbia (Figure 4d). The weaker and westerly expanded AL during the LIG (Figure 5f) is characteristic of a neutral-to-strong negative Pacific Decadal Oscillation/positive North Pacific Index (−PDO/+NPI) phase (Anderson et al., 2016). However, winter half-year sea surface temperatures (SST) in the Pacific Ocean are warmer overall during the LIG relative to the PI, which may obscure any clear PDO signal in LIG-PI SST anomalies (Figure S7 in Supporting Information S1). Additionally, the relationship between the strength of the AL and high latitude hydroclimate is complicated and the longitudinal position of the AL center during -PDO/+NPI states can be highly variable (Anderson et al., 2016; Rodionov et al., 2007). So, given the small magnitude of the LIG winter rainfall anomalies in Alaska and western Canada, the importance of the strength and position of the AL for LIG high latitude hydroclimate is somewhat ambiguous.

In the Atlantic, the moderate strengthening of the LIG latitudinal SLP gradient may indicate a slight preference for a more positive North Atlantic Oscillation (+NAO), which is associated with a steepening of the longitudinal Atlantic SLP gradient (Hurrell, 1995) and an enhancement of westerly flow (Rogers, 1990), during the LIG. While LIG winter half-year SSTs are higher across the entire Atlantic relative to the PI, the highest magnitude positive anomalies occur in the subpolar region, consistent with a preference for a positive Atlantic Meridional Oscillation (AMO) during the LIG (Ruiz-Barradas et al., 2013). A slight negative correlation exists between NAO and total winter precipitation in New England (e.g., Ning & Bradley, 2015) and other parts of the northeastern US today (e.g., Morin et al., 2008), where the ensemble subset produces dry winter half-year rainfall anomalies during the LIG. The dry LIG anomalies extend throughout most of Canada in the ensemble subset winter half-year, but the correlation between NAO and modern total winter precipitation is less clear in eastern Canada (Bonsal & Shabbar, 2008; Chartrand & Pausata, 2020). In the southeast US, the moderate northeasterly wind vector anomalies during the LIG winter half-year in the Gulf of Mexico and extending into Florida (Figure 5f) may contribute to the wet anomalies across the southeast US during the winter half-year observed in the subset ensemble (Figure 4d). This observation is consistent with observations of increased fall rainfall in the region during the 20th-century (Bishop et al., 2018).

The subtropical negative anomalies in the Atlantic Ocean during the summer half-year indicate a weakening of the NASH during the LIG, especially in the eastern Atlantic where the anomalies are largest (Figure 5e). A weakened and northward shifted NASH is associated with the warm phase of the AMO, which has been shown to drive decreased modern rainfall across the central US via diminished advection of moist, maritime air into the continental interior (Hu et al., 2011). Like the winter half-year SSTs, the highest magnitude positive SST anomalies during the summer half-year occur in the subpolar latitudes and off the west coast of Africa, again indicating a preference for +NAO during the LIG. This +NAO preference is consistent with the dry summer half-year anomalies in the central US in the ensemble subset (Figure 4c). The warm phase of the AMO is also associated with enhanced easterly and northeasterly onshore flow to the southeastern US and increased summertime rainfall (Hu et al., 2011), which is reflected in the ensemble subset summer half-year easterly wind vector anomalies (Figure 5e) and positive rainfall anomalies (Figure 4c). Florida is the exception in that it is drier in the LIG ensemble subset. This may be related to the displacement of the tropical easterlies that flow south of the NASH, which leads to diminished advection of moist, unstable air to Florida and drier conditions (Coleman, 1988; Labosier & Quiring, 2013). This matches the pattern of summer half-year aridity in Florida and the Gulf of Mexico in the ensemble subset (Figure 4c) and the splitting of easterly wind vector anomalies to the north and south around Florida (Figure 5e).

Importantly, local thermodynamic forcing may also contribute to greater LIG rainfall through intensification of the hydrologic cycle (Huntington et al., 2018), especially in the northern latitudes where the enhanced seasonality of the LIG drove the largest degree of summer warming. While the clearest influence of warming on the hydrologic cycle is likely increased evaporative demand (Dai et al., 2018), it may also drive an intensification of major oceanic moisture sources for continental precipitation, especially for North America (Gimeno et al., 2013), and contribute to the observed and simulated LIG precipitation patterns.

### 4.3. The Last Interglacial and Future Moisture Patterns

Comparisons between climate model simulations and proxy data from forcing scenarios that are outside the bounds of the PI or historical period are critical for the evaluation of the newest generation of models (Tierney et al., 2020). However, the utility of using large ensembles of past and future climate model simulations can be limited because a lack of robust agreement between different models produces inconclusive results across key

regions (e.g., Cook et al., 2020; Scussolini et al., 2019). Our approach aids in navigating around this problem by providing a rationale to consider a particular subset of models based on the degree of agreement with proxy records for past time periods. Regardless of whether the LIG is an appropriate analog for low end 21st century radiative forcing scenarios (Burke et al., 2018), the subset of models that most closely agree with proxies during warm states like the LIG may provide more informative projections of near-future precipitation patterns relative to the full ensemble.

The enhanced short-wave radiative forcing of the LIG and long-wave radiative forcing of the SSP2-4.5 and SSP5-8.5 simulations produce similar annual precipitation patterns in some regions of North America in the ensemble subset. Both sets of simulations show increases in annual precipitation in high latitudes and decreases in the southern Great Plains relative to the PI. The eastern US is also wetter in both the LIG and the SSP simulations, though this response is of greater magnitude and expands further westward in the SSP simulations. However, the SSP simulations show wetter annual conditions in the Pacific Northwest, Northern Rockies, and upper Great Plains where the LIG is characterized by increased aridity, and drier conditions in the southwest US where the LIG simulations show wet anomalies (Figures 3b, 6a, and 6d).

During the summer half-year, the dry anomalies in the western US and wet anomalies in the eastern US and along the Pacific coast of Mexico are similar in both simulations (Figures 4c, 6b, and 6e). However, the sign of precipitation anomalies during the LIG winter half-year is largely opposite that of the SSP simulations, with enhanced LIG wetness in southwestern North America and aridity across the central and northeastern US and Canada where the SSP simulations show strong dry and wet anomalies respectively (Figures 4d, 6c, and 6f).

These comparisons indicate that the core of the North American Monsoon may strengthen in response to both increased long- and short-wave radiative forcing, though its spatial extent may not expand. Additionally, both the enhanced short-wave radiative forcing of the LIG and the enhanced long-wave radiative forcing of the SSP simulations drive wetter conditions in high latitudes during the summer months, possibly indicating a strong thermal control on the hydrologic in regions like northern Canada and Alaska. However, the disparity in precipitation patterns during the winter half-year between the two forcing scenarios demonstrates that the negative winter insolation anomalies of the LIG drove hydrologic responses that are not comparable to those likely to occur in the coming decades when the radiative forcing will be consistent year-round.

Ultimately, the differences between the orbitally controlled radiative forcing of the LIG and the enhanced greenhouse effect of the end 21st century means that alignment between the moisture patterns of the LIG and SSP simulations is perhaps not to be expected. It may be the case that other climate states from deeper time, like the Pliocene or Eocene which are characterized by greenhouse gas concentrations comparable to or higher than those of the present, provide closer analogs for near future warming (Burke et al., 2018). Even so, our quantitative comparisons between an updated and expanded LIG proxy compilation and the newest generation of PMIP simulations can aid in the evaluation of the Earth system models that we rely on for projecting future climate states that are beyond the range of the PI or historical records that models are often tuned to (Tierney et al., 2020).

## 5. Conclusions

We present comparisons between updated MH and LIG moisture-sensitive proxy compilations and model output from the latest generation of PMIP simulations to assess agreement during the two most recent intervals when NH temperatures were warmer than the PI.

We find low overall agreement between our new and expanded MH proxy compilations and PMIP4 MH simulations, with most models producing the opposite sign and/or smaller magnitude MH precipitation anomalies than demonstrated by the proxy compilation. These findings are consistent with previous comparisons between PMIP simulations and North American moisture-sensitive proxy records (Braconnot et al., 2012; Harrison et al., 2015, 2016; Hermann et al., 2018) and point toward the presence of unconstrained biases or non-linearities in the proxy records and/or the importance of climate feedbacks that are not fully represented in model simulations for NA hydroclimate during the MH.

Agreement between our LIG proxy compilation and PMIP4 simulations is higher than for the MH and we find that an ensemble subset of the three models that agree most closely with the proxy compilation generates the highest AC value overall. The ensemble subset agrees with proxy records in subregions where the full ensemble

does not, namely the Pacific Northwest, Rocky Mountains, northern Mississippi River Basin, and coastal southeastern US, and may thus offer insights that the full ensemble does not. We then use this ensemble subset to assess the seasonal patterns of LIG precipitation, with a key finding being that the NAM may have been strengthened, but not significantly expanded northward during the LIG, and that the wet anomalies of southern California LIG proxy records were primarily driven by increased southwesterly wintertime rainfall, as opposed to summertime monsoonal rainfall.

We find that shifts in the semi-permanent pressure systems in the Atlantic and Pacific during the LIG may have impacted the amount and seasonal distribution of precipitation in much of North America. Specifically, we observe a weakening of the winter half-year LIG latitudinal SLP gradient in the Pacific and a strengthening and northward displacement of the summer half-year LIG Pacific and Atlantic SLP gradients, with important implications for moisture transport and the seasonal and spatial distribution of simulated LIG precipitation anomalies across North America.

SSP simulations of end 21st century hydroclimate from the three models that agree most closely with the LIG proxy compilations suggest that end-21st century precipitation patterns will not closely resemble those of the LIG due to differences in the type and seasonality of the respective forcings. However, our updated proxy compilations and proxy-model comparison offer a tool for benchmarking climate models and their performance in simulating climate states that are warmer than modern conditions.

## Data Availability Statement

Sources for the MH and LIG proxy records used in the model–proxy comparisons are available in Table S1 and S2 respectively and the data are available for download from the NOAA National Climatic Data Center's Paleoclimatology database (https://www.ncei.noaa.gov/access/paleo-search/). Model output is archived through the CMIP5 Data Portal (https://esgf-node.llnl.gov/search/cmip6/). Citations for the models used in this study are available in Table S3 in Supporting Information S1. An example version of the R script used to calculate the Gwet's AC coefficients for proxy compilation-model comparisons has been archived with Zenodo.org (de Wet et al., 2023).

**Acknowledgments**
This work was supported by NSF grants AGS-1554998, and AGS-2102884 to J.L.O; and AGS-2102901 to D.E.I. We thank the three anonymous reviewers for their comments that strengthened the manuscript.

## References

Adam, D. P., & West, G. J. (1983). Temperature and precipitation estimates through the last glacial cycle from Clear Lake, California, pollen data. *Science*, *219*(4581), 168–170. https://doi.org/10.1126/science.219.4581.168

Anderson, L., Berkelhammer, M., Barron, J. A., Steinman, B. A., Finney, B. P., & Abbott, M. B. (2016). Lake oxygen isotopes as recorders of North American Rocky Mountain hydroclimate: Holocene patterns and variability at multi-decadal to millennial time scales. *Global and Planetary Change*, *137*, 131–148. https://doi.org/10.1016/j.gloplacha.2015.12.021

Anderson, R. S., Jiménez-Moreno, G., Ager, T., & Porinchu, D. F. (2014). High-elevation paleoenvironmental change during MIS 6–4 in the central Rockies of Colorado as determined from pollen analysis. *Quaternary Research*, *82*(3), 542–552. https://doi.org/10.1016/j.yqres.2014.03.005

Baker, R. G. (1986). Sangamonian(?) and Wisconsinan paleoenvironments in Yellowstone National Park. *GSA Bulletin*, *97*(6), 717–736. https://doi.org/10.1130/0016-7606(1986)97<717:sawpiy>2.0.co;2

Balch, D. P., Cohen, A. S., Schnurrenberger, D. W., Haskell, B. J., Valero Garces, B. L., Beck, J. W., et al. (2005). Ecosystem and paleohydrological response to quaternary climate change in the Bonneville Basin, Utah. *Palaeogeography, Palaeoclimatology, Palaeoecology*, *221*(1), 99–122. https://doi.org/10.1016/j.palaeo.2005.01.013

Baldini, L. M., Baldini, J. U. L., McElwaine, J. N., Frappier, A. B., Asmerom, Y., Liu, K., et al. (2016). Persistent northward North Atlantic tropical cyclone track migration over the past five centuries. *Scientific Reports*, *6*(1), 37522. https://doi.org/10.1038/srep37522

Bartlein, P. J., Anderson, K. H., Anderson, P. M., Edwards, M. E., Mock, C. J., Thompson, R. S., et al. (1998). Paleoclimate simulations for North America over the past 21,000 years: Features of the simulated climate and comparisons with paleoenvironmental data. *Quaternary Science Reviews*, *17*(6), 549–585. https://doi.org/10.1016/S0277-3791(98)00012-2

Bartlein, P. J., Harrison, S. P., Brewer, S., Connor, S., Davis, B. A. S., Gajewski, K., et al. (2011). Pollen-based continental climate reconstructions at 6 and 21 ka: A global synthesis. *Climate Dynamics*, *37*(3), 775–802. https://doi.org/10.1007/s00382-010-0904-1

Bartlein, P. J., Harrison, S. P., & Izumi, K. (2017). Underlying causes of Eurasian midcontinental aridity in simulations of mid-Holocene climate. *Geophysical Research Letters*, *44*(17), 9020–9028. https://doi.org/10.1002/2017GL074476

Bigelow, N. H., Edwards, M. E., Elias, S. A., Hamilton, T. D., & Schweger, C. E. (2014). Tundra and boreal forest of interior Alaska during terminal MIS 6 and MIS 5e. *Vegetation History and Archaeobotany*, *23*(3), 177–193. https://doi.org/10.1007/s00334-013-0425-z

Binney, H., Edwards, M., Macias-Fauria, M., Lozhkin, A., Anderson, P., Kaplan, J. O., et al. (2017). Vegetation of Eurasia from the last glacial maximum to present: Key biogeographic patterns. *Quaternary Science Reviews*, *157*, 80–97. https://doi.org/10.1016/j.quascirev.2016.11.022

Bishop, D. A., Williams, A. P., Seager, R., Fiore, A. M., Cook, B. I., Mankin, J. S., et al. (2018). Investigating the causes of increased 20(th)-century fall precipitation over the southeastern United States. *Journal of Climate*, *32*(2), 575–590. https://doi.org/10.1175/JCLI-D-18-0244.1

Bonsal, B., & Shabbar, A. (2008). Impacts of large-scale circulation variability on low streamflows over Canada: A review. *Canadian Water Resources Journal / Revue Canadienne Des Ressources Hydriques*, *33*(2), 137–154. https://doi.org/10.4296/cwrj3302137

Braconnot, P., Harrison, S. P., Kageyama, M., Bartlein, P. J., Masson-Delmotte, V., Abe-Ouchi, A., et al. (2012). Evaluation of climate models using palaeoclimatic data. *Nature Climate Change*, *2*(6), 417–424. https://doi.org/10.1038/nclimate1456

Brierley, C. M., Zhao, A., Harrison, S. P., Braconnot, P., Williams, C. J. R., Thornalley, D. J. R., et al. (2020). Large-scale features and evaluation of the PMIP4-CMIP6 *midHolocene* simulations. *Climate of the Past*, *16*(5), 1847–1872. https://doi.org/10.5194/cp-16-1847-2020

Burke, K. D., Williams, J. W., Chandler, M., Haywood, A., Lunt, D., & Otto-Bliesner, B. (2018). Pliocene and Eocene provide best analogs for near-future climates. *Proceedings of the National Academy of Sciences*, *115*(52), 13288–13293. https://doi.org/10.1073/pnas.1809600115

Capron, E., Govin, A., Feng, R., Otto-Bliesner, B. L., & Wolff, E. W. (2017). Critical evaluation of climate syntheses to benchmark CMIP6/PMIP4 127 ka Last Interglacial simulations in the high-latitude regions. *Quaternary Science Reviews*, *168*, 137–150. https://doi.org/10.1016/j.quascirev.2017.04.019

Cárdenes-Sandí, G. M., Shadik, C. R., Correa-Metrio, A., Gosling, W. D., Cheddadi, R., & Bush, M. B. (2019). Central American climate and microrefugia: A view from the last interglacial. *Quaternary Science Reviews*, *205*, 224–233. https://doi.org/10.1016/j.quascirev.2018.12.021

Chartrand, J., & Pausata, F. S. R. (2020). Impacts of the North Atlantic Oscillation on winter precipitations and storm track variability in southeast Canada and the Northeast United States. *Weather and Climate Dynamics*, *1*(2), 731–744. https://doi.org/10.5194/wcd-1-731-2020

Coleman, J. (1988). Climatic warming and increased summer aridity in Florida, U.S.A. *Climatic Change*, *12*(2), 165–178. https://doi.org/10.1007/BF00138937

Conroy, J. L., Karamperidou, C., Grimley, D. A., & Guenthner, W. R. (2019). Surface winds across eastern and midcontinental North America during the Last Glacial Maximum: A new data-model assessment. *Quaternary Science Reviews*, *220*(August), 14–29. https://doi.org/10.1016/j.quascirev.2019.07.003

Cook, B. I., Mankin, J. S., Marvel, K., Williams, A. P., Smerdon, J. E., & Anchukaitis, K. J. (2020). Twenty-First century drought projections in the CMIP6 forcing scenarios. *Earth's Future*, *8*(6), e2019EF001461. https://doi.org/10.1029/2019EF001461

Curry, B. B., & Baker, R. G. (2000). Palaeohydrology, vegetation, and climate since the late Illinois episode (~130 ka) in south-central Illinois. *Palaeogeography, Palaeoclimatology, Palaeoecology*, *155*(1), 59–81. https://doi.org/10.1016/S0031-0182(99)00094-2

Dai, A. (2006). Precipitation characteristics in Eighteen Coupled Climate Models. *Journal of Climate*, *19*(18), 4605–4630. https://doi.org/10.1175/JCLI3884.1

Dai, A., Zhao, T., & Chen, J. (2018). Climate change and drought: A precipitation and evaporation perspective. *Current Climate Change Reports*, *4*(3), 301–312. https://doi.org/10.1007/s40641-018-0101-6

Dalmonech, D., Zaehle, S., Schürmann, G., Brovkin, V., Reick, C., & Schnur, R. (2015). Separation of the effects of land and climate model errors on simulated contemporary land carbon cycle trends in the MPI Earth System Model version 1. *Journal of Climate*, *28*(1), 272–291. https://doi.org/10.1175/JCLI-D-13-00593.1

Delire, C., Levis, S., Bonan, G., Foley, J., Coe, M., & Vavrus, S. (2002). Comparison of the climate simulated by the CCM3 coupled to two different land-surface models. *Climate Dynamics*, *19*(8), 657–669. https://doi.org/10.1007/s00382-002-0255-7

de Wet, C. B., Ibarra, D. E., Belanger, B. K., & Oster, J. L. (2023). North American hydroclimate during past warms states: A proxy compilation-model comparison for the Last Interglacial and the mid-Holocene (version v1). [Software]. Zenodo. https://doi.org/10.5281/zenodo.7992324

Diem, J. E. (2013). Influences of the Bermuda High and atmospheric moistening on changes in summer rainfall in the Atlanta, Georgia region, USA. *International Journal of Climatology*, *33*(1), 160–172. https://doi.org/10.1002/joc.3421

Di Nezio, P. N., & Tierney, J. E. (2013). The effect of sea level on glacial Indo-Pacific climate. *Nature Geoscience*, *6*(6), 485–491. https://doi.org/10.1038/ngeo1823

Dutton, A., Carlson, A. E., Long, A. J., Milne, G. A., Clark, P. U., DeConto, R., et al. (2015). Sea-level rise due to polar ice-sheet mass loss during past warm periods. *Science*, *349*(6244), aaa4019. https://doi.org/10.1126/science.aaa4019

Feng, R., Bhattacharya, T., Otto-Bliesner, B. L., Brady, E. C., Haywood, A. M., Tindall, J. C., et al. (2022). Past terrestrial hydroclimate sensitivity controlled by Earth system feedbacks. *Nature Communications*, *13*(1), 1–11. https://doi.org/10.1038/s41467-022-28814-7

Forester, R. M., Lowenstein, T. K., & Spencer, R. J. (2005). An ostracode based paleolimnologic and paleohydrologic history of Death Valley: 200 to 0 ka. *GSA Bulletin*, *117*(11–12), 1379–1386. https://doi.org/10.1130/B25637.1

Gavin, D., & Brubaker, L. (2015). Late Pleistocene and Holocene environmental change on the Olympic Peninsula, Washington. *Ecological Studies*, *222*. https://doi.org/10.1007/978-3-319-11014-1

Gimeno, L., Nieto, R., Drumond, A., Castillo, R., & Trigo, R. (2013). Influence of the intensification of the major oceanic moisture sources on continental precipitation. *Geophysical Research Letters*, *40*(7), 1443–1450. https://doi.org/10.1002/grl.50338

Glover, K. C., MacDonald, G. M., Kirby, M. E., Rhodes, E. J., Stevens, L., Silveira, E., et al. (2017). Evidence for orbital and North Atlantic climate forcing in alpine Southern California between 125 and 10 ka from multi-proxy analyses of Baldwin Lake. *Quaternary Science Reviews*, *167*, 47–62. https://doi.org/10.1016/j.quascirev.2017.04.028

Grayson, D. K. (2000). Mammalian responses to Middle Holocene climatic change in the Great Basin of the Western United States. *Journal of Biogeography*, *27*(1), 181–192. https://doi.org/10.1046/j.1365-2699.2000.00383.x

Greve, P., Orlowsky, B., Mueller, B., Sheffield, J., Reichstein, M., & Seneviratne, S. I. (2014). Global assessment of trends in wetting and drying over land. *Nature Geoscience*, *7*(10), 716–721. https://doi.org/10.1038/ngeo2247

Gwet, K. (2016). Testing the difference of correlated agreement coefficients for statistical significance. *Educational and Psychological Measurement*, *76*(4), 609–637. https://doi.org/10.1177/0013164415596420

Gwet, K. L. (2008). Computing inter-rater reliability and its variance in the presence of high agreement. *British Journal of Mathematical and Statistical Psychology*, *61*(1), 29–48. https://doi.org/10.1348/000711006X126600

Hardt, B., Rowe, H. D., Springer, G. S., Cheng, H., & Edwards, R. L. (2010). The seasonality of east central North American precipitation based on three coeval Holocene speleothems from southern West Virginia. *Earth and Planetary Science Letters*, *295*(3), 342–348. https://doi.org/10.1016/j.epsl.2010.04.002

Harrison, S. P., Bartlein, P. J., Izumi, K., Li, G., Annan, J., Hargreaves, J., et al. (2015). Evaluation of CMIP5 palaeo-simulations to improve climate projections. *Nature Climate Change*, *5*(8), 735–743. https://doi.org/10.1038/nclimate2649

Harrison, S. P., Bartlein, P. J., & Prentice, I. C. (2016). What have we learnt from palaeoclimate simulations? *Journal of Quaternary Science*, *31*(4), 363–385. https://doi.org/10.1002/jqs.2842

Harrison, S. P., Kutzbach, J.-E., Liu, Z., Bartlein, P. J., Otto-Bliesner, B., Muhs, D., et al. (2003). Mid-Holocene climates of the Americas: A dynamical response to changed seasonality. *Climate Dynamics*, *20*(7–8), 663–688. https://doi.org/10.1007/s00382-002-0300-6

Hermann, N. W., Oster, J. L., & Ibarra, D. E. (2018). Spatial patterns and driving mechanisms of mid-Holocene hydroclimate in Western North America. *Journal of Quaternary Science*, *33*(4), 421–434. https://doi.org/10.1002/jqs.3023

Heusser, L. E. (2000). Rapid oscillations in Western North America vegetation and climate during oxygen isotope stage 5 inferred from pollen data from Santa Barbara Basin (Hole 893A). *Palaeogeography, Palaeoclimatology, Palaeoecology*, *161*(3), 407–421. https://doi.org/10.1016/S0031-0182(00)00096-1

Hu, Q., Feng, S., & Oglesby, R. J. (2011). Variations in North American summer precipitation driven by the Atlantic Multidecadal Oscillation. *Journal of Climate*, *24*(21), 5555–5570. https://doi.org/10.1175/2011JCLI4060.1

Huntington, T. G., Weiskel, P. K., Wolock, D. M., & McCabe, G. J. (2018). A new indicator framework for quantifying the intensity of the terrestrial water cycle. *Journal of Hydrology*, *559*, 361–372. https://doi.org/10.1016/j.jhydrol.2018.02.048

Hurrell, J. W. (1995). Decadal trends in the North Atlantic Oscillation. *Science (New York, N.Y.)*, *269*(5224), 676–679. https://doi.org/10.1126/science.269.5224.676

Ibarra, D. E., Oster, J. L., Winnick, M. J., Caves Rugenstein, J. K., Byrne, M. P., & Chamberlain, C. P. (2018). Warm and cold wet states in the Western United States during the Pliocene–Pleistocene. *Geology*, *46*(4), 355–358. https://doi.org/10.1130/G39962.1

Jiménez-Moreno, G., Scott Anderson, R., & Fawcett, P. J. (2007). Orbital- and millennial-scale vegetation and climate changes of the past 225ka from Bear Lake, Utah–Idaho (USA). *Quaternary Science Reviews*, *26*(13), 1713–1724. https://doi.org/10.1016/j.quascirev.2007.05.001

Knight, C., Dorale, J., & Edwards, R. (2006). *Stalagmite records of interglacial and glacial flooding at Crevice Cave, Missouri, USA*. AGU Fall Meeting Abstracts.

Kwiecien, O., Braun, T., Brunello, C. F., Faulkner, P., Hausmann, N., Helle, G., et al. (2022). What we talk about when we talk about seasonality – A transdisciplinary review. *Earth-Science Reviews*, *225*, 103843. https://doi.org/10.1016/j.earscirev.2021.103843

Labosier, C. F., & Quiring, S. M. (2013). Hydroclimatology of the southeastern USA. *Climate Research*, *57*(2), 157–171. https://doi.org/10.3354/cr01166

Larrasoaña, J. C., Roberts, A. P., & Rohling, E. J. (2013). Dynamics of Green Sahara periods and their role in hominin evolution. *PLoS One*, *8*(10), e76514. https://doi.org/10.1371/journal.pone.0076514

Li, W., Li, L., Fu, R., Deng, Y., & Wang, H. (2011). Changes to the North Atlantic subtropical high and its role in the intensification of summer rainfall variability in the Southeastern United States. *Journal of Climate*, *24*(5), 1499–1506. https://doi.org/10.1175/2010JCLI3829.1

LIGA members, Anderson, P., Borisova, O., de Beaulieu, J.-L., de Vernal, A., Eiriksson, J., et al. (1991). Report of 1st discussion group: The last interglacial in high latitudes of the Northern Hemisphere: Terrestrial and marine evidence. *Quaternary International*, *10–12*, 9–28. https://doi.org/10.1016/1040-6182(91)90038-P

Limoges, A., de Vernal, A., & Van Nieuwenhove, N. (2014). Long-term hydrological changes in the northeastern Gulf of Mexico (ODP-625B) during the Holocene and late Pleistocene inferred from organic-walled dinoflagellate cysts. *Palaeogeography, Palaeoclimatology, Palaeoecology*, *414*, 178–191. https://doi.org/10.1016/j.palaeo.2014.08.019

Lindstrom, S. (1990). Submerged tree stumps as indicators of mid-Holocene aridity in the Lake Tahoe region. *Journal of California and Great Basin Anthropology*, *12*(2), 146–157. Retrieved from http://www.jstor.org/stable/10.2307/27825419

Lora, J. M., & Ibarra, D. E. (2019). The North American hydrologic cycle through the last deglaciation. *Quaternary Science Reviews*, *226*, 105991. https://doi.org/10.1016/j.quascirev.2019.105991

Lyle, M., Heusser, L., Ravelo, C., Andreasen, D., Olivarez Lyle, A., & Diffenbaugh, N. (2010). Pleistocene water cycle and eastern boundary current processes along the California continental margin. *Paleoceanography*, *25*(4). https://doi.org/10.1029/2009PA001836

Marcott, S. A., Shakun, J. D., Clark, P. U., & Mix, A. C. (2013). A reconstruction of regional and global temperature for the past 11,300 years. *Science*, *339*(6124), 1198–1201. https://doi.org/10.1126/science.1228026

Mauri, A., Davis, B. A. S., Collins, P. M., & Kaplan, J. O. (2014). The influence of atmospheric circulation on the mid-Holocene climate of Europe: A data–model comparison. *Climate of the Past*, *10*(5), 1925–1938. https://doi.org/10.5194/cp-10-1925-2014

Members, C. L. I. P. (2006). Last Interglacial Arctic warmth confirms polar amplification of climate change. *Quaternary Science Reviews*, *25*(13), 1383–1400. https://doi.org/10.1016/j.quascirev.2006.01.033

Metcalfe, S. E., Barron, J. A., & Davies, S. J. (2015). The Holocene history of the North American Monsoon: "known knowns" and "known unknowns" in understanding its spatial and temporal complexity. *Quaternary Science Reviews*, *120*, 1–27. https://doi.org/10.1016/j.quascirev.2015.04.004

Miller, I. M., Pigati, J. S., Scott Anderson, R., Johnson, K. R., Mahan, S. A., Ager, T. A., et al. (2014). Summary of the Snowmastodon project special volume: A high-elevation, multi-proxy biotic and environmental record of MIS 6–4 from the Ziegler reservoir fossil site, Snowmass Village, Colorado, USA. *Quaternary Research*, *82*(3), 618–634. https://doi.org/10.1016/j.yqres.2014.07.004

Montero-Serrano, J.-C., Bout-Roumazeilles, V., Carlson, A. E., Tribovillard, N., Bory, A., Meunier, G., et al. (2011). Contrasting rainfall patterns over North America during the Holocene and Last Interglacial as recorded by sediments of the northern Gulf of Mexico. *Geophysical Research Letters*, *38*(14). https://doi.org/10.1029/2011GL048194

Morin, J., Block, P., Rajagopalan, B., & Clark, M. (2008). Identification of large scale climate patterns affecting snow variability in the eastern United States. *International Journal of Climatology*, *28*(3), 315–328. https://doi.org/10.1002/joc.1534

Muhs, D. R., Ager, T. A., & Begét, J. E. (2001). Vegetation and paleoclimate of the last interglacial period, central Alaska. *Quaternary Science Reviews*, *20*(1), 41–61. https://doi.org/10.1016/S0277-3791(00)00132-3

Ning, L., & Bradley, R. (2015). Winter climate extremes over the Northeastern United States and Southeastern Canada and teleconnections with large-scale modes of climate variability. *Journal of Climate*, *28*(6), 2475–2493. https://doi.org/10.1175/JCLI-D-13-00750.1

Osman, M. B., Tierney, J. E., Zhu, J., Tardif, R., Hakim, G. J., King, J., & Poulsen, C. J. (2021). Globally resolved surface temperatures since the Last Glacial Maximum. *Nature*, *599*(7884), 239–244. https://doi.org/10.1038/s41586-021-03984-4

Oster, J. L., Ibarra, D. E., Winnick, M. J., & Maher, K. (2015). Steering of westerly storms over Western North America at the Last Glacial Maximum. *Nature Geoscience*, *8*(3), 201–205. https://doi.org/10.1038/ngeo2365

Otto-Bliesner, B., Braconnot, P., Harrison, S., Lunt, D., Abe-Ouchi, A., Albani, S., et al. (2017). The PMIP4 contribution to CMIP6 – Part 2: Two interglacials, scientific objective and experimental design for Holocene and Last Interglacial simulations. *Geoscientific Model Development*, *10*(11), 3979–4003. https://doi.org/10.5194/gmd-10-3979-2017

Otto-Bliesner, B. L., Brady, E. C., Zhao, A., Brierley, C. M., Axford, Y., Capron, E., et al. (2021). Large-scale features of Last Interglacial climate: Results from evaluating the lig127k simulations for the Coupled Model Intercomparison Project (CMIP6)-Paleoclimate Modeling Intercomparison Project (PMIP4). *Climate of the Past*, *17*(1), 63–94. https://doi.org/10.5194/cp-17-63-2021

PAGES Hydro2k Consortium. (2017). Comparing proxy and model estimates of hydroclimate variability and change over the Common Era. *Climate of the Past*, *13*, 1851–1900. https://doi.org/10.5194/cp-13-1851-2017

Pausata, F. S. R., Emanuel, K. A., Chiacchio, M., Diro, G. T., Zhang, Q., Sushama, L., et al. (2017). Tropical cyclone activity enhanced by Sahara greening and reduced dust emissions during the African humid period. *Proceedings of the National Academy of Sciences*, *114*(24), 6221–6226. https://doi.org/10.1073/pnas.1619111114

Pausata, F. S. R., Zhang, Q., Muschitiello, F., Lu, Z., Chafik, L., Niedermeyer, E. M., et al. (2017). Greening of the Sahara suppressed ENSO activity during the mid-Holocene. *Nature Communications*, *8*(1), 16020. https://doi.org/10.1038/ncomms16020

Pewe, T. L., Berger, G. W., Westgate, J. A., Brown, P. M., & Leavitt, S. W. (1997). Eva interglaciation forest bed, unglaciated East-Central Alaska: Global warming 125,000 years ago. In T. L. Péwé, G. W. Berger, J. A. Westgate, P. M. Brown, & S. W. Leavitt (Eds.), *Eva interglaciation*

*forest bed, unglaciated east-central Alaska: Global warming 125,000 years ago* (Vol. 319, pp. 1–54). Geological Society of America. https://doi.org/10.1130/0-8137-2319-1.1

Piao, J., Chen, W., Wang, L., Pausata, F. S. R., & Zhang, Q. (2020). Northward extension of the East Asian summer monsoon during the mid-Holocene. *Global and Planetary Change*, *184*, 103046. https://doi.org/10.1016/j.gloplacha.2019.103046

Pierce, K. L., Muhs, D. R., Fosberg, M. A., Mahan, S. A., Rosenbaum, J. G., Licciardi, J. M., & Pavich, M. J. (2011). A loess–paleosol record of climate and glacial history over the past two glacial–interglacial cycles (~150ka), southern Jackson Hole, Wyoming. *Quaternary Research*, *76*(1), 119–141. https://doi.org/10.1016/j.yqres.2011.03.006

Pisias, N. G., Mix, A. C., & Heusser, L. (2001). Millennial scale climate variability of the northeast Pacific Ocean and northwest North America based on radiolaria and pollen. *Quaternary Science Reviews*, *20*(14), 1561–1576. https://doi.org/10.1016/S0277-3791(01)00018-X

Prentice, I. C., Jolly, D., & Participants, B. 6000 (2000). Mid-Holocene and Glacial-Maximum vegetation geography of the Northern Continents and Africa. *Journal of Biogeography*, *27*(3), 507–519. https://doi.org/10.1046/j.1365-2699.2000.00425.x

PRISM Climate Group, Oregon State University. (2020). Data created December 2020. Data accessed December 29, 2020. Retrieved from https://prism.oregonstate.edu

Reheis, M. C., Bright, J., Lund, S. P., Miller, D. M., Skipp, G., & Fleck, R. J. (2012). A half-million-year record of paleoclimate from the Lake Manix Core, Mojave Desert, California. *Palaeogeography, Palaeoclimatology, Palaeoecology*, *365–366*, 11–37. https://doi.org/10.1016/j.palaeo.2012.09.002

Riboulleau, A., Bout-Roumazeilles, V., & Tribovillard, N. (2014). Controls on detrital sedimentation in the Cariaco Basin during the last climatic cycle: Insight from clay minerals. *Quaternary Science Reviews*, *94*, 62–73. https://doi.org/10.1016/j.quascirev.2014.04.023

Rodionov, S. N., Bond, N. A., & Overland, J. E. (2007). The Aleutian Low, storm tracks, and winter climate variability in the Bering Sea. *Deep Sea Research Part II: Topical Studies in Oceanography*, *54*(23), 2560–2577. https://doi.org/10.1016/j.dsr2.2007.08.002

Rogers, J. (1990). Patterns of low-frequency monthly sea level pressure variability (1899–1986) and associated wave cyclone frequencies. *Journal of Climate*, *3*(12), 1364–1379. https://doi.org/10.1175/1520-0442(1990)003<1364:POLFMS>2.0.CO;2

Ruiz-Barradas, A., Nigam, S., & Kavvada, A. (2013). The Atlantic Multidecadal Oscillation in twentieth century climate simulations: Uneven progress from CMIP3 to CMIP5. *Climate Dynamics*, *41*(11), 3301–3315. https://doi.org/10.1007/s00382-013-1810-0

Scheff, J. (2018). Drought indices, drought impacts, $CO_2$, and warming: A historical and geologic perspective. *Current Climate Change Reports*, *4*(2), 202–209. https://doi.org/10.1007/s40641-018-0094-1

Schmidt, M. W., & Spero, H. J. (2011). Meridional shifts in the marine ITCZ and the tropical hydrologic cycle over the last three glacial cycles. *Paleoceanography*, *26*(1). https://doi.org/10.1029/2010PA001976

Schweger, C. E., & Matthews, J. V. (1991). The last (Koy-Yukon) interglaciation in the Yukon: Comparisons with holocene and interstadial pollen records. *Quaternary International*, *10–12*, 85–94. https://doi.org/10.1016/1040-6182(91)90042-M

Scussolini, P., Bakker, P., Guo, C., Stepanek, C., Zhang, Q., Braconnot, P., et al. (2019). Agreement between reconstructed and modeled boreal precipitation of the Last Interglacial. *Science Advances*, *5*(11), eaax7047. https://doi.org/10.1126/sciadv.aax7047

Scussolini, P., Eilander, D., Sutanudjaja, E. H., Ikeuchi, H., Hoch, J. M., Ward, P. J., et al. (2020). Global river discharge and floods in the warmer climate of the Last Interglacial. *Geophysical Research Letters*, *47*(18), e2020GL089375. https://doi.org/10.1029/2020GL089375

Sharpe, S. E., & Bright, J. (2014). A high-elevation MIS 5 hydrologic record using mollusks and ostracodes from Snowmass Village, Colorado, USA. *Quaternary Research*, *82*(3), 604–617. https://doi.org/10.1016/j.yqres.2014.01.014

Springer, G. S., Rowe, H. D., Hardt, B., Cheng, H., & Edwards, R. L. (2014). East central North America climates during marine isotope stages 3–5. *Geophysical Research Letters*, *41*(9), 3233–3237. https://doi.org/10.1002/2014GL059884

Steinman, B. A., Pompeani, D. P., Abbott, M. B., Ortiz, J. D., Stansell, N. D., Finkenbinder, M. S., et al. (2016). Oxygen isotope records of Holocene climate variability in the Pacific Northwest. *Quaternary Science Reviews*, *142*, 40–60. https://doi.org/10.1016/j.quascirev.2016.04.012

Suh, Y. J., Diefendorf, A. F., Freimuth, E. J., & Hyun, S. (2020). Last interglacial (MIS 5e) and Holocene paleohydrology and paleovegetation of midcontinental North America from Gulf of Mexico sediments. *Quaternary Science Reviews*, *227*, 106066. https://doi.org/10.1016/j.quascirev.2019.106066

Sun, W., Wang, B., Zhang, Q., Pausata, F. S. R., Chen, D., Lu, G., et al. (2019). Northern Hemisphere land monsoon precipitation increased by the Green Sahara during Middle Holocene. *Geophysical Research Letters*, *46*(16), 9870–9879. https://doi.org/10.1029/2019GL082116

Sundqvist, H. S., Kaufman, D. S., McKay, N. P., Balascio, N. L., Briner, J. P., Cwynar, L. C., et al. (2014). Arctic Holocene proxy climate database – New approaches to assessing geochronological accuracy and encoding climate variables. *Climate of the Past*, *10*(4), 1605–1631. https://doi.org/10.5194/cp-10-1605-2014

Swain, D. L., Tsiang, M., Haugen, M., Singh, D., Charland, A., Rajaratnam, B., & Diffenbaugh, N. S. (2014). The extraordinary California drought of 2013/2014: Character, context, and the role of climate change. *Bulletin of the American Meteorological Society*, *95*(9), S3–S7. Retrieved from http://proxy.library.vanderbilt.edu/login?url=https://www.proquest.com/scholarly-journals/extraordinary-california-drought-2013-2014/docview/1623231385/se-2?accountid=14816

Swann, A. L. S., Fung, I. Y., Liu, Y., & Chiang, J. C. H. (2014). Remote vegetation feedbacks and the Mid-Holocene Green Sahara. *Journal of Climate*, *27*(13), 4857–4870. https://doi.org/10.1175/JCLI-D-13-00690.1

Tabor, C., Otto-Bliesner, B., & Liu, Z. (2020). Speleothems of South American and Asian Monsoons influenced by a Green Sahara. *Geophysical Research Letters*, *47*(22), e2020GL089695. https://doi.org/10.1029/2020GL089695

Tarnocai, C. (1990). Paleosols of the interglacial climates in Canada. *Géographie Physique et Quaternaire*, *44*(3), 363–374. https://doi.org/10.7202/032836ar

Teed, R. (2000). A >130,000-year-long pollen record from Pittsburg Basin, Illinois. *Quaternary Research*, *54*(2), 264–274. https://doi.org/10.1006/qres.2000.2161

Thompson, A. J., Zhu, J., Poulsen, C. J., Tierney, J. E., & Skinner, C. B. (2022). Northern Hemisphere vegetation change drives a Holocene thermal maximum. *Science Advances*, *8*(15), eabj6535. https://doi.org/10.1126/sciadv.abj6535

Thompson, R., Whitlock, C., Bartlein, P., & Al, E. (1993). Climatic changes in the Western United States since 18,000 yr B.P. In H. Wright, J. Kutzbackm, I. Webb, T. W. Ruddiman, S.-P. FA, & P. Bartlein (Eds.), *Global climates since the last glacial maximum* (pp. 468–513). University of Minnesota Press.

Tierney, J. E., Pausata, F. S. R., & de Menocal, P. B. (2017). Rainfall regimes of the Green Sahara. *Science Advances*, *3*(1), e1601503. https://doi.org/10.1126/sciadv.1601503

Tierney, J. E., Poulsen, C. J., Montañez, I. P., Bhattacharya, T., Feng, R., Ford, H. L., et al. (2020). Past climates inform our future. *Science*, *370*(6517), eaay3701. https://doi.org/10.1126/science.aay3701

Tingstad, A., Groves, D., & Lempert, R. (2014). Paleoclimate scenarios to inform decision making in water resource management: Example from Southern California's Inland Empire. *Journal of Water Resources Planning and Management*, *140*(10), 4014025. https://doi.org/10.1061/(ASCE)WR.1943-5452.0000403

Trenberth, K. E. (2011). Changes in precipitation with climate change. *Climate Research*, *47*(1–2), 123–138. https://doi.org/10.3354/cr00953

Turney, C. S. M., & Jones, R. T. (2010). Does the Agulhas Current amplify global temperatures during super-interglacials? *Journal of Quaternary Science*, *25*(6), 839–843. https://doi.org/10.1002/jqs.1423

Turney, C. S. M., Jones, R. T., McKay, N. P., van Sebille, E., Thomas, Z. A., Hillenbrand, C.-D., & Fogwill, C. J. (2020). A global mean sea surface temperature dataset for the Last Interglacial (129–116 ka) and contribution of thermal expansion to sea level change. *Earth System Science Data*, *12*(4), 3341–3356. https://doi.org/10.5194/essd-12-3341-2020

Whitlock, C., & Bartlein, P. J. (1997). Vegetation and climate change in northwest America during the past 125 kyr. *Nature*, *388*(6637), 57–61. https://doi.org/10.1038/40380

Wise, E. K. (2016). Five centuries of U.S. West Coast drought: Occurrence, spatial distribution, and associated atmospheric circulation patterns. *Geophysical Research Letters*, *43*(9), 4539–4546. https://doi.org/10.1002/2016GL068487

Wong, C. I., Potter, G. L., Montañez, I. P., Otto-Bliesner, B. L., Behling, P., & Oster, J. L. (2016). Evolution of moisture transport to the Western U.S. during the last deglaciation. *Geophysical Research Letters*, *43*(7), 3468–3477. https://doi.org/10.1002/2016GL068389

Woodhouse, C., Lukas, J., Morino, K., Meko, D., & Hirschboeck, K. (2016). Using the past to plan for the future—the value of paleoclimate reconstructions for water resource planning (pp. 161–182). https://doi.org/10.1201/b19534-12

Woolfenden, W. B. (2003). A 180,000-year pollen record from Owens Lake, CA: Terrestrial vegetation change on orbital scales. *Quaternary Research*, *59*(3), 430–444. https://doi.org/10.1016/S0033-5894(03)00033-4

Wyatt, P. (1990). Amino acid evidence indicating two or more ages of pre-Holocene nonglacial deposits in Hudson Bay Lowland, Northern Ontario. *Géographie Physique et Quaternaire*, *44*(3), 389–393. https://doi.org/10.7202/032838ar

## References From the Supporting Information

Boucher, O., Servonnat, J., Albright, A. L., Aumont, O., Balkanski, Y., Bastrikov, V., et al. (2020). Presentation and evaluation of the IPSL-CM6A-LR Climate Model. *Journal of Advances in Modeling Earth Systems*, *12*(7), e2019MS002010. https://doi.org/10.1029/2019MS002010

Cao, J., Wang, B., Yang, Y.-M., Ma, L., Li, J., Sun, B., et al. (2018). The NUIST Earth System Model~(NESM) version 3: Description and preliminary evaluation. *Geoscientific Model Development*, *11*(7), 2975–2993. https://doi.org/10.5194/gmd-11-2975-2018

Danabasoglu, G., Lamarque, J.-F., Bacmeister, J., Bailey, D. A., DuVivier, A. K., Edwards, J., et al. (2020). The Community Earth System Model Version 2 (CESM2). *Journal of Advances in Modeling Earth Systems*, *12*(2), e2019MS001916. https://doi.org/10.1029/2019MS001916

Decharme, B., Delire, C., Minvielle, M., Colin, J., Vergnes, J.-P., Alias, A., et al. (2019). Recent changes in the ISBA-CTRIP land surface system for use in the CNRM-CM6 Climate Model and in global off-line hydrological applications. *Journal of Advances in Modeling Earth Systems*, *11*(5), 1207–1252. https://doi.org/10.1029/2018MS001545

Giorgetta, M. A., Jungclaus, J., Reick, C. H., Legutke, S., Bader, J., Böttinger, M., et al. (2013). Climate and carbon cycle changes from 1850 to 2100 in MPI-ESM simulations for the Coupled Model Intercomparison Project phase 5. *Journal of Advances in Modeling Earth Systems*, *5*(3), 572–597. https://doi.org/10.1002/jame.20038

Guo, C., Bentsen, M., Bethke, I., Ilicak, M., Tjiputra, J., Toniazzo, T., et al. (2019). Description and evaluation of NorESM1–F: A fast version of the Norwegian Earth System Model (NorESM). *Geoscientific Model Development*, *12*, 343–362. https://doi.org/10.5194/gmd-12-343-2019

Hajima, T., Watanabe, M., Yamamoto, A., Tatebe, H., Noguchi, M. A., Abe, M., et al. (2020). Development of the MIROC-ES2L Earth system model and the evaluation of biogeochemical processes and feedbacks. *Geoscientific Model Development*, *13*(5), 2197–2244. https://doi.org/10.5194/gmd-13-2197-2020

Kelley, M., Schmidt, G. A., Nazarenko, L. S., Bauer, S. E., Ruedy, R., Russell, G. L., et al. (2020). GISS-E2.1: Configurations and climatology. *Journal of Advances in Modeling Earth Systems*, *12*(8), e2019MS002025. https://doi.org/10.1029/2019MS002025

Kuhlbrodt, T., Jones, C. G., Sellar, A., Storkey, D., Blockley, E., Stringer, M., et al. (2018). The low-resolution version of HadGEM3 GC3.1: Development and evaluation for global climate. *Journal of Advances in Modeling Earth Systems*, *10*(11), 2865–2888. https://doi.org/10.1029/2018MS001370

Seland, Ø., Bentsen, M., Olivié, D., Toniazzo, T., Gjermundsen, A., Graff, L. S., et al. (2020). Overview of the Norwegian Earth System Model (NorESM2) and key climate response of CMIP6 DECK, historical, and scenario simulations. *Geoscientific Model Development*, *13*(12), 6165–6200. https://doi.org/10.5194/gmd-13-6165-2020

Sidorenko, D., Rackow, T., Jung, T., Semmler, T., Barbi, D., Danilov, S., et al. (2015). Towards multi-resolution global climate modeling with ECHAM6–FESOM. Part I: Model formulation and mean climate. *Climate Dynamics*, *44*(3), 757–780. https://doi.org/10.1007/s00382-014-2290-6

Voldoire, A., Saint-Martin, D., Sénési, S., Decharme, B., Alias, A., Chevallier, M., et al. (2019). Evaluation of CMIP6 DECK experiments with CNRM-CM6-1. *Journal of Advances in Modeling Earth Systems*, *11*(7), 2177–2213. https://doi.org/10.1029/2019MS001683

Volodin, E. M., Mortikov, E. V., Kostrykin, S. V., Galin, V. Y., Lykossov, V. N., Gritsun, A. S., et al. (2018). Simulation of the modern climate using the INM-CM48 climate model. *Russian Journal of Numerical Analysis and Mathematical Modelling*, *33*(6), 367–374. https://doi.org/10.1515/rnam-2018-0032

Williams, K. D., Copsey, D., Blockley, E. W., Bodas-Salcedo, A., Calvert, D., Comer, R., et al. (2018). The Met Office Global Coupled Model 3.0 and 3.1 (GC3.0 and GC3.1) configurations. *Journal of Advances in Modeling Earth Systems*, *10*(2), 357–380. https://doi.org/10.1002/2017MS001115

Yukimoto, S., Kawai, H., Koshiro, T., Oshima, N., Yoshida, K., Urakawa, S., et al. (2019). The Meteorological Research Institute Earth System Model version 2.0, MRI-ESM2.0: Description and basic evaluation of the physical component. *Journal of the Meteorological Society of Japan. Series II*, *97*(5), 931–965. https://doi.org/10.2151/jmsj.2019-051

Zhang, Q., Berntell, E., Axelsson, J., Chen, J., Han, Z., de Nooijer, W., et al. (2021). Simulating the mid-Holocene, last interglacial and mid-Pliocene climate with EC-Earth3-LR. *Geoscientific Model Development*, *14*(2), 1147–1169. https://doi.org/10.5194/gmd-14-1147-2021

Zheng, W., Yu, Y., Luan, Y., Zhao, S., He, B., Dong, L., et al. (2020). CAS-FGOALS datasets for the two interglacial Epochs of the Holocene and the Last Interglacial in PMIP4. *Advances in Atmospheric Sciences*, *37*(10), 1034–1044. https://doi.org/10.1007/s00376-020-9290-8

Ziehn, T., Chamberlain, M. A., Law, R. M., Lenton, A., Bodman, R. W., Dix, M., et al. (2020). The Australian Earth System Model: ACCESS-ESM1.5. *Journal of Southern Hemisphere Earth Systems Science*, *70*(1), 193–214. https://doi.org/10.1071/ES19035